

Changes in the shape of cloud ice water content vertical structure due to aerosol variations,
by Steven T. Massie, Julien Delanoë, Charles G. Bardeen, Jonathan Jiang and Lei Huang

Reviewer #1

This study addresses the question of effect of aerosols on the invigoration of deep tropical clouds. They regard an enhancement of the ice water content (IWC) as an indicator for the invigoration. While invigoration can certainly increase the IWC, the IWC was shown to be potentially enhanced also by microphysical effects of the added aerosols. Fan et al. (2013) showed that larger numbers of smaller ice particles fall more slowly and therefore enhance the IWC. This has to be added to introduction.

The revised paper now discusses Fan et al (2013) in the Introduction in a new paragraph. The paper by Morrison and Grabowski (2011) is also discussed in the new paragraph added to the revised paper.

Major comments:

1. The main response parameters are poorly defined. Please define clearly IWCsum, IWCreg and IWCshape with equations and allocate for that explanation a figure with illustration. Please state the units.

The revised paper has equations 1-3 which define the IWCsum, IWCreg and IWCshape profiles. Newly added Figure 4 of the revised paper summarizes the processing steps. The units are stated for each set of profiles.

2. The authors conclude that cloud adjacency does not affect much their conclusions. The data that they show to support that is not very convincing. The obvious way to show this is to repeat the final results for the various adjacency thresholds, and see the extent that it affects these results. Sample size should not be an issue for the final results shown in Figures 8 and 9.

The revised paper now includes a new figure (Figure 8) which presents means from the previous Figures 8 and 9, as a function of the cloud pixel-distance value. New Figure 8 indicates that cloud-adjacency has a minor effect on the previous Figures 8 and 9 mean values.

3. It is not clear to me how Figure 1 was constructed. It appears that more profiles were averaged towards the larger numbers on the abscissa, because they converge towards ordinate value of zero. How was that done? Were the profiles binned and averaged in some way?

Assuming that the question is in regard to the construction of Figure 5 of the original paper (Figure 7 in revised paper), the x axis value is the number of profiles that is

associated with a specific region and season that is associated with the corresponding derivative on the y axis. When Figure7 is first discussed in the revised paper, we add the following sentence to clarify the Figure's construction: "As explained in Section 3 (Step 4 processing), the value of the IWC_{reg} derivative for a 2 km altitude bin is the average of two derivatives, based upon IWC_{reg} values at the first and second, and first and third, aerosol bins".

4. The authors state that "three AOD bins (i.e. 0.05 - 0.15, 0.15-0.35, 0.35 – 0.45), were chosen to represent low, medium, and high amounts of AODs". By doing this the authors ignored the two main properties of aerosol effects on cloud invigoration, as described in two papers in Science: (Koren et al., 2008; Rosenfeld et al., 2008). First, the cloud invigoration responds to the logarithm of the aerosols concentrations. Second, the effect saturates at AOD of 0.25 to 0.3, and may reverse at larger AOD. This is evident in Figure 3, where there is large difference between the lines of AOD 1 and 2, but bins 2 and 3 are practically the same. The authors have to expand the introduction to include the discussion of the aerosols effect, as mentioned here. Furthermore, the analysis has to be redone with re-binning accordingly. The cases with $AOD < 0.05$ are the cleanest and thus expected to have the greatest contrast to the polluted cases. Based on the principle of the logarithmic effect, the difference between $AOD < 0.05$ and AOD of 0.05 to 0.15 should be larger than what the authors found between bins 1 and 2 in the present version,. Why did the authors exclude $AOD < 0.05$? This should be a bin on its own, which I expect to be the most informative. In summary, for the paper to be considered for publication in ACP it has to undergo a major revision. The background has to be rewritten with a more physical basis, the methodology has to be clarified, the analyses have to be completely redone with new binning, the effects of adjacency effect have to be tested on the final results, and the discussion of the results has to commensurate with the newly written physical background.

- a) The 0.05 is a typo introduced into the original paper (we apologize for this). The aerosol bins used in the calculations of the original paper, and reported in the figures of the original paper, are 0.01 - 0.15, 0.15-0.30, 0.30 – 0.45. Figure 3 of the original paper has the correct lower bound (0.01) of the first AOD bin range. These three sets of AODs are based upon an examination of probability distribution functions of MODIS AODs such that there are approximately an equal number of AODs for the three aerosol bin ranges. We tried to have the statistics of the three AOD bins to be similar. Since the expected errors (see page 9, lines 5-6, of the revised paper) for MODIS C6 AODs over the Ocean are -0.02 (-10%) and +0.04 (+10%) and over Land by $\pm (0.05 +15\%)$, a separate bin range (i.e. 0.01 – 0.05) would apply MODIS data of low accuracy.
- b) Table 1 was added to the revised paper to state the AOD, AAOD, and CO bins clearly. Reviewer 2 suggested that OMI AAODs and MLS CO data be added to the study, and we did this in the revised paper.
- c) A new paragraph is added to the Introduction of the revised paper which discusses Koren et al. (2008) and Rosenfeld et al. (2008) in regard to saturation effects. Inhibition effects are also discussed in a new paragraph,

- 1 with reference to papers by Ramanathan et al. (2005, 2007) who modeled and
2 observed the stabilizing effects of absorptive aerosol offshore of India. These
3 four papers form the basis of the added written physical background.
- 4 d) Equations 1-3 clarify the methodology (i.e. how the IWCsum, IWCreg and
5 IWCshape values are calculated).
 - 6 e) The reviewers' requested binning (i.e. lower bound is less than 0.05 for the
7 first bin) is actually the original binning.
 - 8 f) New Figure 8 illustrates the effects of cloud adjacency on the final results
9 (original Figures 8 and 9, Figures 11 and 12 in revised paper). Curves of the
10 means for the All AOD, 2, and 4 pixel-distance AOD fields, are presented in
11 Figure 8 as requested by the reviewer. This Figure is placed in the text when
12 Table 2 (previous Table 1 listing of the pdf means) is first discussed. It is
13 apparent from Figure 8 in the revised paper that the cloud adjacency issue did
14 not have a large impact upon our particular calculations.
 - 15 g) Additional text has been added in the Introduction and Discussion in regard to
16 the added written physical background. Table 4 has been added to the text
17 which indicates the percent of MODIS observations for which invigoration
18 and inhibition scenarios are apparent. The saturation scenario in the MODIS
19 data is present twice as often as the inhibition scenario.

20
21 I did not comment on minor issues, because they likely will not survive the revision, if
22 done as I expect it to be.

23
24 References:

- 25
26 Fan J., L. R. Leung, D. Rosenfeld, Q. Chen, Z. Li, J. Zhang, H. Yan, 2013: Microphysical
27 effects determine macrophysical response for aerosol impacts on deep convective
28 clouds. *Proceedings of the National Academy of Sciences*, 110(48), E4581-E4590.
29
30 Koren, I., Martins, J. V., Remer, L. A., & Afargan, H. (2008). Smoke invigoration versus
31 inhibition of clouds over the Amazon. *science*, 321(5891), 946-949.
32
33 Rosenfeld, D., Lohmann, U., Raga, G. B., O'Dowd, C. D., Kulmala, M., Fuzzi, S., ...
34 & Andreae, M. O. (2008). Flood or drought: how do aerosols affect precipitation?.
35 *science*, 321(5894), 1309-1313.

36
37 All of these papers are included in the revised paper.

38
39 Interactive comment on *Atmos. Chem. Phys. Discuss.*, doi:10.5194/acp-2015-732, 2016.
40

Changes in the shape of cloud ice water content vertical structure due to aerosol variations,
by Steven T. Massie, Julien Delanoë, Charles G. Bardeen, Jonathan Jiang and Lei Huang

Anonymous Referee #2

Received and published: 16 February 2016

This paper is generally well written. After addressing my major concern below, the
results of this paper would undoubtedly motivate worthwhile future research efforts in
this field.

My major concern is that this study uses only MODIS AOT to analyze vertical structure
changes of ice clouds under various AOT amounts. It is noted that MODIS can not
distinguish aerosol types. While aerosols could perturb the vertical profiles of clouds
via cloud particle size change and latent heat release, and thus invigorate convection
(Rosenfeld, 2008), absorptive aerosols could result in less solar radiation at the surface
and more stable vertical temperature profile and thus inhibit cloud development (see
work by Ramanathan 2005, 2007). I noted in most cases different aerosol types are
mixed, which may explain why only very small changes of cloud vertical structure were
found by this study. My suggestions is to expand the database to include OMI absorp-
tive aerosols, or perhaps Aura MLS CO (the newest version 4) and thus the cases for
absorbing aerosols can be identified and distinguished.

We agree that analysis that compares the effects of both absorptive aerosol (OMI
AAOD and 215 hPa MLS CO, an absorptive aerosol proxy) and MODIS AODs (which
include both scattering and absorptive aerosol) is an important task.

In the revised paper additional text and figures have been added to include
calculations in which absorptive aerosol (OMI AAOD and MLS V4 CO at 215 hPa) data
is used in the same manner as the MOIS AODs.

As discussed in the revised paper, the calculations (see Figure 15 and Figure 13)
are supportive of the assertion that absorptive aerosol tends to inhibit cloud development.
Figures 15 and 13 graphically illustrate differences between the effects of absorbing
aerosols (from OMI and MLS) and all aerosols (from MODIS). This is especially
apparent in comparing the positive MODIS AOD means and negative MLS CO means.

Minor comments:

(1) Figure 1. The reason for conducting the study in 12 different regions should be
explained more clearly. For example, the regions can be defined by cloud dynamics,
which varies from region to region.

Text on page 109 has been revised to indicate that topographical and surface
heating characteristics vary from region to region.

The 12 regions were selected to cover the tropics, selected to separate ocean from
land, and selected to include as many IWC profiles as possible in order to reinforce the
statistics.

1
2 (2) Figure 5, and also page 12 Line 7. You mentioned the largest derivatives are over
3 India, why?
4

5 As stated in the text, the variance in the derivatives (new Figure 7) increases as
6 the number of profiles decreases. India has the smallest area of the 12 regions. We
7 believe that this is why India primarily has the largest spread in the derivatives.

8 Text has been added (page 15 of revised paper) to also mention the fact that India
9 is subject to complicated monsoon dynamics, and the “elevated heat pump” physics of
10 William Lau likely also is of importance. Absorptive aerosol above the Tibetan plateau is
11 attributed to provide an elevated heating source which leads to enhanced circulation that
12 will draw air from the surface upwards along the southern flank of the Himalayas. India
13 likely is subject to some of the most complicated aerosol-cloud interactions as anyplace
14 in the world.
15

16 Also, how derivatives in the 12 regions differ?
17

18 Text on page 17 (revised paper) discusses the spatial variations (revised paper
19 lines 5-8, page 17) and seasonal variations (revised paper lines 24-29, page 17) of the
20 derivatives.
21

22 (3) I also suggest the authors to analyze the vertical velocity field in each of the 12
23 regions using MERRA data, which could provide additional information.
24

25 We agree that additional calculations in regard to the cloud dynamic variables is
26 an important task. For completeness, such a study should examine several dynamic
27 variables: the vertical velocity field, wind shear, relative humidity, and CAPE, on a
28 region by region basis.

29 A concern we do have in such a study is that models and observations need not
30 necessarily agree in spatial and temporal agreement in regard to the location and timing
31 of cloud development. This task is deserving of careful analysis but we feel it is
32 substantially outside the scope of the present study which in its revised form is already
33 long in length.
34

35 Interactive comment on Atmos. Chem. Phys. Discuss., doi:10.5194/acp-2015-732, 2016.
36
37

Changes in the shape of cloud ice water content vertical structure due to aerosol variations

Steven T. Massie^{1,3}, Julien Delanoë², ~~and~~ Charles G. Bardeen³, Jonathan Jiang and Lei Huang⁴

[1]{Laboratory for Atmospheric and Space Physics, Boulder, Colorado}

[2]{LATMOS/IPSL/UVSQ/CNRS, Guyancourt, France}

[3]{National Center for Atmospheric Research, Boulder, Colorado}

[4]{Jet Propulsion Laboratory, Pasadena, California}

Correspondence to: S. T. Massie (Steven.Massie@lasp.colorado.edu)

Abstract

Changes in the shape of cloud ice water content (IWC) vertical structure due to ~~aerosol~~ variations in Moderate Resolution Imaging Spectroradiometer (MODIS) aerosol optical depths (AODs), Ozone Monitoring Instrument (OMI) absorptive aerosol optical depths (AAODs), and Microwave Limb Sounder (MLS) CO (an absorptive aerosol proxy) at 215 hPa, are calculated in the Tropics during 2007-2010 based upon an analysis of DARDAR ~~ice water content (IWC)~~ profiles for deep convective clouds. DARDAR profiles are a joint retrieval of CloudSat-CALIPSO data. ~~Our analysis~~ Analysis is performed for 12 separate regions over land and ocean, and carried out applying ~~Moderate Resolution Imaging Spectroradiometer (MODIS) aerosol optical depth (AOD)~~ fields that attempt to correct for 3D cloud adjacency effects. The 3D cloud adjacency effects have a small impact upon our particular calculations of aerosol-cloud indirect effects. IWC profiles are averaged for

three AOD bins individually for the 12 regions. The IWC average profiles are also normalized to unity at 5 km altitude in order to study changes in the *shape* of the average IWC profiles as AOD increases. Derivatives of the IWC average profiles, and derivatives of the IWC shape profiles, in percent change per 0.1 change in MODIS AOD units, are calculated separately for each region. Means of altitude-specific probability distribution functions, which include both ocean and land IWC shape regional derivatives, are modest, near 5%, and positive to the 2σ level between 11 and 15 km altitude. Similar analyses is carried out for three AAOD and three CO bins. On average, the vertical profiles of the means of the derivatives based upon the profile shapes over land and ocean are smaller for the profiles binned according to AAOD and CO values, than for the MODIS AODs, which include both scattering and absorptive aerosol. This difference in character supports the assertion that absorptive aerosol can inhibit cloud development.

Formatted: Font: Italic

1 Introduction

Uncertainty in aerosol effects upon clouds remains the largest of the global climate forcing uncertainties (Stocker et al., 2013). Tao et al. (2012) discuss the various types of aerosol indirect effects (e.g. effects on cloud droplets and ice particles, reflectance, cloud heights, lifetime, coverage, and precipitation). Though various aerosol indirect effects have been identified, there remains much quantitative uncertainty.

By the cloud invigoration mechanism (Rosenfeld et al., 2008), an increase in aerosol is expected to modify the manner in which vertical and horizontal cloud structure develops in deep convective clouds. The cloud invigoration mechanism is of fundamental importance in regard to aerosol indirect effects upon deep convective clouds. It is expected that the vertical ice water content (IWC), particle radii, and heating rate profiles of a deep convective cloud ~~differs~~*differ* under low and high aerosol optical depths (AODs) due to different initial cloud condensation nuclei (CCN) values in the lower portion of the cloud. A change in the CCN concentration alters the formation rate and size of liquid droplets, allowing more water to be transported above the freezing level, which leads to a perturbed

vertical profile of latent heat release, and subsequent invigoration of cloud development. This invigoration effect will occur throughout the cloud, changing IWC vertical structure.

The literature of observed and modeled aerosol indirect effects, however, is characterized by a variety of conclusions with differences in even the *sign* of the effects. For example, Koren et al. (2010) analyzed Moderate-Resolution Imaging Spectroradiometer (MODIS) AOD and cloud top pressure data for July – August 2007 over the Atlantic west of equatorial Africa for low and high clouds. For high clouds near 370 hPa (i.e. 7 km altitude, see Figure 6 of Koren et al., 2010), cloud top pressure changed by -7% / 0.1 AOD (i.e. cloud top heights *increased* as AOD increased). In this paper we use % change per 0.1 AOD units in order to compare the calculations from several studies. Assuming that the cloud top position is dependent upon the location of cloud vertical optical depths near unity, a decrease in cloud top pressure corresponds to moving the optical depth profile upwards in altitude. IWC is then +7% / 0.1 AOD larger at the position of the higher cloud top. In contrast, Wall, Zipser, and Liu (2014) studied congestus (4-8 km altitude range), analyzing 14 years of Tropical Rainfall Measuring Mission (TRMM) radar precipitation features, and 6 years of CloudSat radar reflectivity data. Aerosol Index (AI) data (i.e. AI is the product of MODIS AOD and the MODIS ~~Angstrom~~Ångström exponent) were collocated with the TRMM and CloudSat data. TRMM echo-top heights *increased* with increasing AI over the Amazon and Africa, and *decreased* over the equatorial Atlantic and southwest United States. Differences in CloudSat maximum reflectivity means of clean and dirty congestus were statistically significant at the 99% level below 4 km over the Amazon, and at 4-5 km over Africa, but *not* at higher altitudes.

It is important to note that changes in particle radius due to changes in aerosol also result in IWC profile perturbations, even in the absence of convective invigoration. Morrison and Grabowski (2011) used a two-dimensional cloud-system resolving model to investigate aerosol indirect effects for pristine, polluted, and highly polluted conditions during a 6 day period of active monsoon conditions. The ensemble calculations indicated a small weakening of convection, higher cloud top heights and anvil ice mixing ratios for the polluted cases. Smaller ice particle sizes and smaller fall velocities perturbed the IWC profiles. Fan et al. (2013) used the NCAR WRF model, coupled to a spectral-bin

Formatted: Font color: Black

1 microphysics code, to simulate deep convective clouds (DCC) for one month for three
2 different regions over the tropical western Pacific (i.e. the TWP-International Cloud
3 Experiment), southern China, and over the U.S. southern Great Plains ARM site. They
4 found “that although the widely accepted theory of DCC invigoration due to aerosol’s
5 thermodynamic effect (additional latent heat release from freezing of greater amount of
6 cloud water) may work during the growing stage, it is microphysical effect influenced by
7 aerosols that drives the dramatic increase in cloud cover, cloud top height, and cloud
8 thickness at the mature and dissipation stages by inducing larger amounts of smaller but
9 longer-lasting ice particles in the stratiform/anvils of DCCs, even when thermodynamic
10 invigoration is absent”.

11 Increases in AOD will invigorate for small AODs, though inhibit convection at larger
12 AODs, since larger AODs decrease the amount of sunlight which reaches the surface.
13 Based upon application of a pseudo-adiabatic parcel model, Rosenfeld et al. (2008)
14 estimated that maximum release of convective energy occurs for AODs near 0.3. The
15 contrasting influences of cloud microphysics and radiative processes, and their influence
16 on cloud fraction were parameterized in analytic equations by Koren et al. (2008), and
17 validated by an analysis of MODIS AODs, cloud fractions, and cloud top pressure observed
18 over the Amazon in the dry season. The upper panel of Figure 2 of Koren et al. (2008)
19 indicates that cloud top pressures are lowest (i.e. cloud top heights are highest) for AODs
20 near 0.4.

21 It is also possible that *absorptive* AOD can *inhibit* cloud development. Ramanathan et al.
22 (2005) used model simulations to study the influence of absorptive aerosol offshore of
23 India. The model aerosol perturbed temperature profile vertical gradients in the first several
24 kilometers near the surface, yielding a stabilizing influence upon cloud development.
25 Ramanathan et al. (2007) deployed small aerial aircraft over the Maldives in 2006 to
26 measure aerosol characteristics during time periods with and without enhanced aerosol
27 amounts. Heating rate calculations indicated that the enhanced aerosol produced a vertical
28 temperature profile that was more stable, and therefore likely inhibited cloud development.

1 According to theory, buoyancy increases by the release of latent heat, and decreases when
2 condensate loading (i.e. the weight of liquid or ice in a fluid parcel) increases (see Eqns
3 2.50 – 2.53 of Houze, 2014). Lebo and Seinfeld (2011) state that “the aerosol-induced
4 effect is controlled by the balance between latent heating and the increase in condensed
5 water aloft, each having opposing effects on buoyancy.” Since changes in buoyancy can
6 be positive or negative, depending upon specific situations in which latent heating or
7 condensate perturbations dominant, changes in cloud structure IWC likely could be
8 positive or negative as AOD increases.

9 Lebo and Seinfeld (2011) modeled aerosol effects on deep convection by applying the
10 Weather Research and Forecasting (WRF) model as a cloud resolving model, with separate
11 bulk and bin microphysics schemes. Figure 6 of Lebo and Seinfeld (2011) presents domain
12 averaged liquid and IWC profiles at 2, 4, and 6 hours for “Clean”, “Semi-Polluted”, and
13 “Polluted” scenarios, with cloud condensation nuclei (CCN) values of 100, 200, and 500
14 cm^{-3} , respectively. The three IWC profiles for the three CCN values are equal to each other
15 at 5 (6) km altitude for the bulk (bin) microphysics schemes, respectively, and then diverge
16 at higher altitudes. This diverging characteristic indicates that the shape of the IWC profile
17 changes as AOD changes. This Figure motivates us to calculate IWC average profiles for
18 individual regions in the Tropics, and IWC *shape* profiles, for several AOD bins. The IWC
19 shape profiles are obtained by normalizing the IWC average profiles to unity at 5 km
20 altitude.

21 There are noticeable differences in the bulk and bin microphysics model calculations in
22 Figure 6 of Lebo and Seinfeld (2011). The bulk scheme IWC profiles differ by – 5% at the
23 IWC peak near 6 km altitude, indicating a decrease in IWC as aerosol increases, while the
24 bin microphysics IWC profiles differ by 120% at the IWC peak near 9 km altitude,
25 indicating a large increase in IWC as aerosol increases. Figure 1 of Rosenfeld et al. (2008),
26 which graphs 500 nm AOD as a function of CCN, can be used to estimate AODs that
27 correspond to the model CCN values. The difference in AOD between the Clean and
28 Polluted CCN values is approximately 0.094. The 120% increase in IWC therefore
29 translates to an increase in IWC of 127% per 0.1 AOD. Lebo and Seinfeld (2011) attribute

the bulk and bin microphysics model differences to differences in vertical motion and particle size (sedimentation) characteristics of the two microphysical schemes.

Storer and van den Heever (2013) modeled deep convective clouds by running the Regional Atmospheric Modeling System (RAMS) (Cotton et al., 2003) in a 2D radiative-convective equilibrium framework. Six CCN loadings between 100 and 3200 cm⁻³ were applied in separate calculations. After a 60 day initialization, model output was sampled every 5 min during a 10 day period. They note that early storm updrafts were influenced by increased latent heating, while more mature updrafts were largely influenced by increased drag from condensate loading. Differences in buoyancy curves for “polluted” and “clean” aerosol cases (see Figure 8 of Storer and van den Heever, 2013) indicate that latent heating effects were numerically smaller, by an order of magnitude, than those due to condensate loading. The number of cloud-top counts, averaged over 10 days, shifted toward higher and medium cloud tops and fewer low cloud tops (see Figure 1 of Storer and van den Heever, 2013). The freezing level was near 4.4 km, with low, medium, and high cloud tops defined for altitudes less than 4.4 km, 4.4–10 km, and altitudes greater than 10 km, respectively. On a percentage basis, medium and high cloud top heights increased by approximately 3% and 5%, respectively, between the 100 and 400 cm⁻³ CCN values. The 100 cm⁻³ and 400 cm⁻³ CCN values are closest in value to those used in the Lebo and Seinfeld (2011) calculations discussed above.

Changes in the *shape* of cloud ice water content vertical structure, and changes in ~~ice-water content~~ (IWC) vertical profiles, due to aerosol variations in Moderate Resolution Imaging Spectroradiometer (MODIS) aerosol optical depths (AODs), Ozone Monitoring Instrument (OMI) absorptive aerosol optical depths (AAODs), and Microwave Limb Sounder (MLS) CO (an absorptive aerosol proxy) at 215 hPa, are calculated in this paper for the Tropics over land and ~~oceans~~ocean during 2007-2010 based upon an analysis of DARDAR IWC profiles of deep convective clouds. DARDAR profiles (Delanoë and Hogan, 2008; Delanoë and Hogan, 2010) are a joint radar-lidar retrieval using CloudSat radar reflectivity and CALIOP lidar observations at 532 nm. We carry out our calculations over several years (2007-2010), individual regions and seasons, in order to build up statistics. Section 2 discusses the data used in our study, Section 3 discusses ~~our~~the Methodology which is

Formatted: Font: Italic

1 [applied in a similar manner to the AOD, AAOD and CO data](#), and results are presented in
2 Section 4. A discussion of the results and conclusions are presented in Section 5.

3 4 **2 Data**

5 Ice water content vertical profiles are from the v2.1.0 DARDAR (raDAR/liDAR) data
6 archive (<http://www.icare.univ-lille1.fr/drupal/archive/>) of the ICARE Thematic Center.
7 The DARDAR cloud product is derived using the Varcloud algorithm (Delanoë and Hogan
8 2008) and utilizes CloudSat reflectivity, and CALIOP lidar backscatter at 532 nm to jointly
9 retrieve the properties of ice clouds (e.g. IWC, visible extinction, effective cloud particle
10 radius). There is one DARDAR profile, with a vertical resolution of 60 m, for every
11 CloudSat radar profile and therefore an along-track horizontal resolution of 1.7 km.
12 Cloudsat (Stephens et al, 2002) and the CALIOP lidar (on the CALIPSO satellite, Winker
13 et al., 2010) were launched in tandem in 2006 as part of the A-Train. We analyze data from
14 all months of 2007 through 2010.

15 The DARDAR retrieval algorithm is discussed in Delanoë and Hogan (2008), Delanoë and
16 Hogan (2010) and in ICARE archive documentation (http://www.icare.univ-lille1.fr/drupal/projects_data/dardar/docs/varcloud_algorithm_description-v1.0.pdf). The
17 applied optimal estimation technique (see Rodgers, 2000 for a general discussion)
18 incorporates up to date aircraft particle size distribution and habit information to formulate
19 forward model look-up tables. The lidar forward model uses a fast radiative transfer code
20 (Hogan 2006). The combination of 95 GHz CloudSat radar and 532 nm CALIOP lidar
21 observations provide information on both small and larger ice particles, since CloudSat and
22 CALIOP are sensitive to larger and smaller particles, respectively. Since the lidar is subject
23 to strong attenuation, the radar measurement takes over for thick ice clouds. The radar-
24 lidar overlap region allows one to retrieve simultaneously size and concentration
25 information. For this reason the combination of the two measurements improves the
26 retrieval of cloud properties compared to single instrument retrievals. The DARDAR data
27 focuses upon ice particles, so our analysis is restricted to altitudes above 5 km.
28

Deng et al. (2013) found reasonable agreement between CloudSat-CALIPSO (2C-ICE) and DARDAR retrieval products. IWC values from 2B-CWC-RO, 2C-ICE, and DARDAR generally are in good agreement, while 2B-CWC-RVOD radii were 40% larger than the 2C-ICE and DARDAR radii.

One stated concern in aerosol-indirect effect studies is that it is difficult to measure aerosol optical depths near clouds using nadir view satellite instruments. A cloud away from an observation point scatters light from the cloud towards the nadir observation point, which is then scattered towards the satellite sensor. Varnai and Marshak (2009) quantified how MODIS reflectance is enhanced as a function of distance to the nearest cloud. The reflectance is enhanced by ~10% when clouds are 5 km away from clear sky footprints at a wavelength of 0.68 μm . Zhang et al. (2005) compared AERONET and MODIS MOD04 AODs. They demonstrate that MODIS AODs are enhanced at cloud edges, with differences between MODIS and AERONET AODs increasing as the cloud fraction increases, while the AERONET values stay relatively constant. We address this concern in our calculations by using the latest V6 MODIS aerosol data that include a parameter indicating the average pixel distance from a measured AOD to the nearest cloud feature.

MODIS version 6 MYD04 data files are used to specify daily aerosol optical depth fields. In particular, we utilize the “Optical_Depth_Land_and_Ocean” AOD values at 0.55 μm , which are specified at 10 km horizontal spatial resolution. We process the 10 km AODs into daily data files at $1^\circ \times 1^\circ$ longitude-latitude resolution for 25° S to 25° N . As discussed by Levy et al. (2013), the Collection 6 (henceforth C6) aerosol retrieval algorithms have made several improvements compared to the C5 data. The C6 “Average_Cloud_Pixel_Distance_Land_Ocean” variable specifies the number of pixel units from an AOD to the nearest cloud pixel. Pixel unit distances are on the order of 0.5 km. We use this variable to calculate separate $1^\circ \times 1^\circ$ AOD fields for several “cloud screening” cases. For the first case, all AODs are used within a $1^\circ \times 1^\circ$ grid box if the AOD is between 10^{-3} and 3. Another set uses all AODs that are e.g. 2 or more pixel units from MODIS clouds. Daily $1^\circ \times 1^\circ$ fields of AODs for 2, 4, and 6 pixel units, and the “all AOD” case, are calculated separately for 25° S to 25° N . As discussed in the next section, the AOD fields are used in separate calculations, for each pixel-distance case, to assess the

sensitivity of the calculations to 3D cloud adjacency effects. The AODs used in our processing are for quality flag 3 (i.e. only the best quality data is used).

Levy et al. (2014) discusses the differences in C6 and C5 Aqua MODIS AODs. C6 AODs increase by 0.05 over the tropical ocean and the Amazon, decrease by -0.05 over the southern oceans and northern mid-latitudes, and increase by 0.02 on a global basis. C6 AODs over ~~the~~ land increased by 0.10 over East Asia, vegetation, Africa, Eastern United States, and decreased over the Western United States, South Africa, and semi-arid regions. The correlations of MODIS and AERONET AODs change slightly from 0.928 to 0.937 for the C5 and C6 data, respectively. Expected errors for C6 AODs over the Ocean are -0.02 (-10%) and +0.04 (+10%) and over ~~the~~ Land by $\pm (0.05 + 15\%)$.

The OMI OMAEROe data are contained in gridded (level 3) hdf files with a resolution of $\frac{1}{4}^\circ \times \frac{1}{4}^\circ$ (http://disc.sci.gsfc.nasa.gov/Aura/data-holdings/OMI/omaeroe_v003.shtml). These data files utilize for each grid cell the level 2 data that has the shortest sun to sensor path length. The data are derived from a multi-wavelength aerosol retrieval algorithm (Veihelmann et al., 2007; Veihelmann and Veeffkind, 2009) that uses 14 bands and a look up reflectance table, calculated for four aerosol model types (desert dust, biomass burning, volcanic, and weakly absorbing aerosol), size distributions, and aerosol layer altitudes. The level 2 data are calculated by minimizing the differences between observed and model reflectance values.

MLS CO (http://disc.sci.gsfc.nasa.gov/uui/datasets/GES_DISC_ML2CO_V004) at 215 hPa is an aerosol proxy (Jiang et al. 2008; Jiang et al. 2009). CO is a byproduct of incomplete combustion of biofuels and fossil fuel, and is associated with soot (which absorbs light). CO is retrieved from microwave radiances in two bands of the 240 GHz radiometer (Livesey et al. 2008). Level 2 version 4.2 profiles have a vertical resolution of 3.5 – 5 km in the upper troposphere. We grid CO measurements at 215 hPa into daily $1^\circ \times 1^\circ$ data files. As discussed in Livesey et al. (2015), 215 hPa is the highest pressure (lowest altitude) for which data applications are recommended. The 215 hPa data has a precision of 19 ppbv and a systematic uncertainty of ± 30 ppbv ($\pm 30\%$)

3 Methodology

Figure 1 presents the various regions in the Tropics for which we calculate average IWC profiles. The 12 regions are either over land or ocean since cloud dynamics differs over land and ocean (Houze, 2014), cloud dynamics likely varies from region to region due to various topographical and surface heating characteristics, and cloud activity peaks at different local times on a regional basis (Liu and Zipser, 2008). We focus on the Tropics in this study to avoid mid-latitude complications due to frontal dynamics. The 12 regions cover most of the Tropics, ~~yet~~ are limited in longitude, ~~i.e. limited~~ and include as many IWC profiles as possible in local times ~~in order to reinforce the A-train observations~~ statistics.

The general distribution of MODIS AOD, OMI AAOD, and MLS CO, averaged over all seasons between 2007 and 2010, is presented in Figure 2. The largest AODs originate from land regions over Africa, South America, Southeast Asia, and Indonesia. There are few 0.55 μm AODs over North Africa. This is due to the large surface albedo of desert sands, for which it is difficult for MODIS to detect suspended aerosols. AODs, AAODs, and CO values are generally larger over land than ocean. Large AODs, AODs, and CO are observed offshore of Africa due to transport of mainland aerosol to the adjacent ocean areas. Absorptive aerosol is prevalent over South American and Africa due to the prevalence of biomass burning in these regions.

An example of the IWC structure of a deep convective cloud, observed near 111° W and 8° N on July 10, 2007, is presented in Figure 23. DARDAR IWC, with original units of Kg / m³ is rescaled for graph clarity purposes. 240 individual profiles were measured in this deep convective cloud. In general, IWC increases in value from the top of the cloud downwards, reaches a maximum value, then decreases somewhat. For this cloudy region, latitude and height variations in IWC are apparent, since the heights of the top of the cloud and the maximum IWC values vary as a function of latitude.

Based upon the original DARDAR data files, we proceed in several steps, processing both day and night profiles. We first process the DARDAR data into daily files of IWC profiles ~~(i.e. IWCdaily)~~. An original profile is retained if the profile has IWC greater than 5×10^{-5}

Kg / m³ and less than 0.05 Kg / m³ (i.e. near the high end of the retrieval) and if the IWC values are contiguous for two or more kilometers in vertical extent. This Step 1 processing is helpful due to the large data volume (i.e. 1.9 TB, 8.2 x 10⁶ profiles for the Tropics) of the original DARDAR data files. This Step and subsequent processing steps are summarized in Figure 4.

The Step 2 processing of the DARDAR and AOD data produces yearly files of deep convective cloud structure for 2007 – 2010. Step 1 profiles are used if the vertical depth of the profile is at least 5 km above 5 km altitude. Step 1 IWC profiles are collocated with the daily MODIS AOD files to calculate IWC_{sum} profile sums, binned according to AOD, longitude, latitude, aerosol to cloud pixel distance, season, and altitude.

$$\text{IWC}_{\text{sum}}(\text{AOD, longitude, latitude, pixel distance, season, altitude}) = \sum \text{IWC}_{\text{daily}} \quad (1)$$

There are three MODIS AOD bins, 72 longitude and 11 latitude bins at 5° resolution, four cloud-screening cases (for “all AOD”, 2, 4, and 6 pixel-distance cases), four seasons, and 131 altitude steps in 0.1 km increments from 5 to 18 km altitude. IWC_{sum} units are in Kg / m³. The three AOD bins stated in Table 1 (i.e. 0.0501 - 0.15, 0.15 - 0.3530, 0.3530 - 0.4572) were chosen to represent low, medium, and high amounts of AODs. Calculation (as indicated by inspection of MODIS AOD probability distribution functions of AODs, PDFs). The MODIS AOD PDFs (not shown) indicated indicate that there are relatively few MODIS AODs greater than 0.45. AAOD and CO bins are also specified in Table 1. The bin ranges were selected from examination of e.g. x=MODIS AOD versus y=OMI AAOD scatter diagrams, which indicated the range of OMI AAOD corresponding to each MODIS AOD bin range. The AOD versus AAOD and AOD versus CO scatter diagrams places the AOD, AAOD, and CO calculations on an approximate equal footing.

The third Step of the processing sorts the IWC_{sum} data into IWC_{reg} regional averages, binned according to AOD, region, aerosol to cloud pixel distance, season, and altitude.

$$\text{IWC}_{\text{reg}}(\text{AOD, region, pixel distance, season, altitude}) =$$

$$\frac{\sum \text{IWC}_{\text{sum}}(\text{AOD, longitude, latitude, pixel distance, season, altitude})}{\text{N}} \quad (2)$$

Formatted: Font: 12 pt, Not Superscript/ Subscript

Formatted: Font: 12 pt, Not Superscript/ Subscript

Formatted: Font: 12 pt, Not Superscript/ Subscript

This calculation averages data into seven altitude bins of 2 km vertical ~~extent~~ extending from 5 to 18 km altitude. IWC_{reg} units are in Kg / m³. The reason for the vertical binning is to promote as much statistical significance as possible from the averaging process. The number of IWC profiles in a single region and altitude bin varies from less than 10³ to greater than 9 x 10⁴ since AODs are generally smaller over the oceans and the regions vary in spatial extent.

We also calculate ~~the shape~~ normalized IWC profiles (i.e. IWC_{shape} of profiles) based upon the IWC_{reg} profiles by dividing the IWC_{reg} profile by the IWC_{reg} value in the 5 to 7 km bin range.

$$\begin{aligned} & \text{IWC}_{\text{shape}}(\text{AOD}, \text{region}, \text{pixel distance}, \text{season}, \text{altitude}) = \\ & \frac{\text{IWC}_{\text{reg}}(\text{AOD}, \text{region}, \text{pixel distance}, \text{season}, \text{altitude})}{\text{IWC}_{\text{reg}}(\text{AOD}, \text{region}, \text{pixel distance}, \text{season}, \text{altitude from 5 to 7 km})} \quad (3) \end{aligned}$$

The IWC_{shape} array, in dimensionless units, has the same binning as the IWC_{reg} array. The IWC_{shape} profile is of course 1.0 for the 5- - 7 km bin, and deviates from unity at higher altitudes, indicating how the shape of the IWC structure progressively changes above 7 km altitude. As noted above, the calculation of the IWC_{shape} profiles is motivated by the profiles displayed in Figure 6 of Lebo and Seinfeld (2011) since modeled IWC profiles for the three model CCN values diverge at altitudes greater than 5 altitude.

Another reason to look at the shape of IWC structure is that observational sampling of a cloudy region for the three AOD bins is not a precisely “controlled” process. A cloudy region has a 3D IWC structure with 3D variations in IWC. The CloudSat and CALIPSO sampling of 3D IWC structures (i.e. a vertical 2D slice through the cloudy region, with a corresponding set of 1°x1° MODIS AODs) is random. One random sampling of a cloudy region could be weighted by more observations with lower IWC values, and another random sampling could be weighted by higher IWC values. If the sampling of a 3D cloudy ~~region~~ regions, with respect to low and high regions of IWC, is not consistently similar for the three bins of AOD, then a sampling issue arises. By looking at the shape of the vertical IWC structure one can attempt to mitigate this sampling issue, by putting the IWC_{reg}

Formatted: Font: 12 pt, Not Superscript/ Subscript

Formatted: Font: 12 pt, Not Superscript/ Subscript

Formatted: Font: 12 pt, Not Superscript/ Subscript

Formatted: Font: 12 pt, Not Superscript/ Subscript

Formatted: Font: 12 pt, Not Superscript/ Subscript

Formatted: Font: 12 pt, Not Superscript/ Subscript

Formatted: Font: 12 pt, Not Superscript/ Subscript

Formatted: Font: 12 pt, Not Superscript/ Subscript

Formatted: Font: 12 pt, Not Superscript/ Subscript

average profiles for the three AOD bins on a normalized footing. It is reasonable to assume that this sampling issue becomes less of a concern when the number of profiles ~~in for~~ a given region and season increases.

In Step 4 of the processing, derivatives are calculated two ways. $\partial IWC_{reg} / \partial AOD$ derivatives (henceforth, IWC_{reg} derivatives) are first calculated for each region, season, and pixel-distance AOD field at each of the seven altitude bins. The value of the IWC_{reg} derivative is the average of two derivatives, based upon IWC_{reg} values at the first and second, and first and third, aerosol bins.

$$\frac{\partial IWC_{reg}}{\partial AOD}(\text{region, season, pixel distance, altitude})$$

$$= 0.5 \{ (IWC_{reg}(2, \dots) - IWC_{reg}(1, \dots)) / (AOD(2) - AOD(1)) + (IWC_{reg}(3, \dots) - IWC_{reg}(1, \dots)) / (AOD(3) - AOD(1)) \} \quad (4)$$

where numbers (e.g. (2)) refer to the AOD bin of Table 1, and ... refers to the region, season, pixel distance, and altitude bins. This average derivative is then transformed, for graphical and other purposes, into percent change ~~in IWC~~ per 0.1 AOD units. ~~In by dividing the second calculation derivative by the average IWCreg value.~~ $\partial IWC_{shape} / \partial AOD$ derivatives ~~are~~ (henceforth, IWC_{shape} derivatives) are then calculated for the seven altitude bins in similar fashion.

Equations (1) – (4) are applied to the IWC profiles using OMI AAOD and MLS CO values, separately, in place of the MODIS AOD data. The transformed AAOD and CO derivatives are in % per 0.02 AAOD and % per 100 ppbv units, respectively. The AAOD and CO derivatives are binned according to region, season, pixel distance, and altitude, in the same way as for the AOD derivatives.

In Step 5 of the processing, we place the IWC_{reg} derivatives for the various regions and seasons into ~~probability distribution functions (PDFs)~~ at each of the seven altitude bins. ~~PDFs are constructed separately from the AOD, AAOD, and CO derivatives.~~ Derivatives are included in the PDF if the number of IWC profiles in a derivative is greater than 10^3 . (The 10^3 threshold was empirically determined based upon visual examination of

Formatted: Font: 12 pt, Not Superscript/ Subscript

Formatted: Font: 12 pt, Not Superscript/ Subscript

Formatted: Font: 12 pt, Not Superscript/ Subscript

Formatted: Font: 12 pt, Not Superscript/ Subscript

Formatted: Font: 12 pt, Not Superscript/ Subscript

Formatted: Font: 12 pt, Not Superscript/ Subscript

1 ~~individual~~ IWC_{reg} profiles). We calculate the means of the PDFs, standard deviations from
2 the means, and 95% (2σ) confidence levels of the means of the PDFs. In a similar manner,
3 the IWC_{shape} derivatives are used to calculate the means of PDFs and 95% confidence
4 limits of the means of the PDFs. As discussed below, we examine and compare the means
5 of the ~~two sets of various~~ PDFs.

6 Finally, an additional separate processing goes back to Step 2 and assigns MODIS AODs
7 at a given $1^\circ \times 1^\circ$ grid box to the AOD at that position using a *randomly* chosen day during
8 the year of interest. Ideally, random AODs should yield means of the PDF of the derivatives
9 that are close to zero, since the $\partial \text{IWC}_{\text{reg}} / \partial \text{AOD}$ and $\partial \text{IWC}_{\text{shape}} / \partial \text{AOD}$ derivatives are
10 reversed in sign if low and high values of AOD are interchanged. We compare the PDF
11 means of this separate processing with those of the previous paragraph.

13 4 Results

14 Figure 35 illustrates the average vertical structure of IWC_{reg} over Africa during summer
15 (June-July-August) and over the southeast Pacific during winter (December-January-
16 February). The mark at 5 km specifies the average between 5 and 7 km altitude, etc. The
17 IWC_{reg} values over Africa increase as AOD increases for nearly every altitude level. In
18 contrast, the IWC_{reg} curves over the southeast Pacific increase from the first to second bin
19 for the 5 to 9 km range, while decreasing for the first and third aerosol bins. These curves
20 illustrate that derivatives for specific regions and seasons can be either positive or negative.

21 These curves also indicate that calculations of derivatives need to be confined to specific
22 regions. There are height differences at which a specific IWC value is observed, e.g. 0.3 g
23 $/ \text{m}^3$ occurs at 11 km over the SE Pacific and at 10.5 km over Africa for the 0.01 – 0.15
24 AOD bin. Global calculations which lump together profiles from different regions mix
25 IWC profiles of different height characteristics, due to regional differences in e.g. cloud
26 type and/or weather conditions. If the number of regional profiles varies from region to
27 region for a specific AOD bin, and these profiles have different average height
28 characteristics, then the derivatives calculated using the globally lumped profiles are prone

Formatted: Font: 12 pt, Not Superscript/ Subscript

Formatted: Font: 12 pt, Not Superscript/ Subscript

Formatted: Font: 12 pt, Not Superscript/ Subscript

Formatted: Font: 12 pt, Not Superscript/ Subscript

Formatted: Font: 12 pt, Not Superscript/ Subscript

to error (since differences in the average regional profiles are related to both AOD effects and regional differences due to cloud type and/or weather conditions).

The impact of cloud adjacency effects upon the AOD fields is illustrated in Figure 46. Daily MODIS C6 AOD data fields were averaged for 25° S to 25° N for “all AOD”, 2, 4, and 6 pixel-distance cases. On the x axis the AODs correspond to the case when all AODs in the 1°x1° grid box are used to define the AOD field. On the y axis is the ratio of the AODs for a particular pixel-distance to the “all AOD” case. The ratios for all of the curves are smallest for the smaller AODs, and increase to larger values as the AODs increase. The AODs are approximately 2% smaller for the 2 pixel-distance case compared to the “all AOD” case. As more and more AODs are tossed out of the screening process, the AOD averages become progressively smaller than the “all AOD” case, up to 8% for the 6 pixel-distance case. Unfortunately, the number of nonzero 1°x1° grid box AODs decreases for the 4 and 6 pixel-distance cases. Use of the 2 pixel-distance field is more practical than the other cases. Since each AOD bin range in our Step 2 binning processing covers a large range in AOD, a 2% effect likely places an “all AOD” and e.g. “2 cloud pixel distance” AOD into the *same* AOD bin range. It is therefore expected that correction for the cloud adjacency effect, using the three AOD bin ranges mentioned above in Section 3, will be of second order in our particular calculations.

In Figure 57 the statistical distribution of AOD, AAOD, and CO IWC_{reg} derivatives for individual regions and seasons, are displayed separately over land and ocean. The x axis indicates the number of individual profiles associated with the derivative, ~~with IWC_{reg} derivatives on the y axis, of a specific region and season, with IWC_{reg} derivatives on the y axis.~~ As explained in Section 3 (Step 4 processing), the value of the IWC_{reg} derivative for a 2 km altitude bin is the average of two derivatives, based upon IWC_{reg} values at the first and second, and first and third, aerosol bins. The absolute magnitude of the derivatives over land or ocean decrease as the number of profiles increases. ~~The largest derivatives are those over mainland India, which are assigned the square symbol in Figure 5. The India land region has the smallest area of our 12 regions.~~

Formatted: Font: 12 pt, Not Superscript/ Subscript

The largest derivatives in the AOD, AAOD, and CO panels are those over mainland India, which are assigned the square symbol in Figure 7. The India land region has the smallest area of our 12 regions, yet is subject to complicated monsoon dynamics, and with the presence of absorptive aerosols over the Tibetan Plateau, likely subject to the absorptive aerosol “elevated heat pump” mechanism (Lau et al. 2006). Absorptive aerosol above the Tibetan plateau is attributed to provide an elevated heating source which leads to enhanced circulation that will draw air from the surface upwards along the southern flank of the Himalayas. India likely is subject to some of the most complicated aerosol-cloud interactions as anyplace in the world.

In calculations presented below, we present analyses in which the largest derivatives are included, and excluded, from the calculations. Derivatives are not used in the exclusionary calculations if the number of profiles in the average are less than 1000 and/or if the derivatives are greater than 100% per 0.10 AOD, 100% per 0.02 AAOD, or 100% per 100 ppbv CO.

Table 42 presents means of the PDFs for the IWC_{reg} derivatives over land and ocean for the 2 km altitude bins, expressed as a function of the pixel-distance value. The means are calculated assigning equal weight to each region (i.e. the calculations are not weighted by the number of profiles observed in each region). The number of statistically significant derivatives (i.e. number of separate regions and seasons) that went into the PDF decreases as the cloud pixel-distance value increases (since the number of AODs in the daily $1^\circ \times 1^\circ$ grid boxes decreases as the pixel-distance value increases). This is most apparent for the 4 pixel-distanced AOD fields. The PDF means in Table 2 are larger over land than the ocean, with fairly small modulation in these means due to pixel-distance choice.

Figure 8 illustrates how the means of curves presented later in the text (i.e. Figures 11 and 12) are sensitive to the pixel-distance value. The means in Figure 8 differ from those in Table 2 since the derivatives, used to calculate the curves in Figures 11 and 12, are those less than 100 % per 0.1 AOD, while all derivatives are included in the Table 2 calculations. The “All AOD” case (i.e. “ALL in Figure 8) and the Screen 2 (i.e. pixel-distance 2 AOD field) set of means are similar in Figure 8.

Formatted: Font: 12 pt, Not Superscript/ Subscript

Overall, it is apparent that the 3D cloud adjacency effect has a fairly small impact upon the means of the PDFs in our calculations. For this reason, we henceforth focus on results for the “all AOD” case in order to maximize the number of derivatives used in our calculations.

The means of the IWC_{reg} derivative PDFs for the “all AOD” case are presented in Figure 6.9 separately for land and ocean data. The 95% confidence (2σ) limits of the means are given by the horizontal lines. Over the ocean, the left panel of Figure 6.9 indicates that the means are consistent with the zero % per 0.1 AOD line, as the zero % line falls between the 95% confidence limits of the means. Over land the means are between 10 and 20 percent for the 9 to 13 km range, also consistent with the 0% line.

Table 2.3 presents means of the PDFs for the IWC_{reg} and IWC_{shape} derivatives over land and ocean for the 2km2 km altitude bins, for the “all AOD” case. As before (see Table 4.2) the PDF IWCs derivative means over ~~the~~ land are larger than those over the ocean, and the values increase with altitude. In addition, the Rnd columns ~~Rnd~~ refer to calculations in which a random day is calculated for each specific day, injecting a random AOD field into the calculations. If AODs are randomly selected from the MODIS AODs, then the ~~final~~ means of the PDFs of the IWC_{shape} derivatives are small, though nonzero. We interpret the nonzero values near 2% as evidence that the means of the *cloud dynamic* variables (e.g. surface humidity, CAPE, surface temperature, etc) are different for the various AOD bins. The fact that the differences in the IWC_{shape} and Rnd columns are positive (especially for the observations over land) indicates, ~~however~~, that the cloud invigoration effect is nonzero and positive.

Examination of individual derivatives over the ocean and land for the various altitude ranges indicates that most regions have positive and negative derivatives. This is consistent with our statements above in the Introduction that buoyancy is perturbed by both positive (latent heat) and negative (condensate loading) influences. There are more positive ocean IWC_{reg} derivatives north than south of the equator, with the largest annually averaged derivatives over the Northwest and Northeast Pacific, and smallest derivatives over the South Atlantic. Largest annually averaged land derivatives are found over India, South America, and Africa, with smallest derivatives over Australia.

Formatted: Font: 12 pt, Not Superscript/ Subscript

Formatted: Not Superscript/ Subscript

Formatted: Font: 12 pt, Not Superscript/ Subscript

Formatted: Font: 12 pt, Not Superscript/ Subscript

Formatted: Font: 12 pt, Not Superscript/ Subscript

1 The means of the IWC_{shape} derivative PDFs for the “all AOD” case are presented in Figure
2 ~~7~~10. Over the ocean and land the means are near 5% and 10% - 20% per 0.1 AOD for the
3 9 to 13 km range, respectively. The derivatives are positive to the 2σ level for the 9 -11
4 and 13-15 km altitude ranges over land (i.e. mean - 95% confidence limit of the mean value
5 is positive for these two altitude ranges).

6 As remarked above, in regard to Figure ~~5~~7, the India averages have a much smaller number
7 of profiles than that for other regions, since the geographical extent of this region is the
8 smallest of the 12 regions. The IWC_{shape} curves, ~~from inspection~~, are noiser than those of
9 the other regions and the derivatives are substantially larger than those for the other regions.
10 For this reason, it is appropriate to present calculations in which ~~the~~ India land derivatives,
11 ~~and those from other regions~~ are excluded-, ~~if the number of profiles in an average is less~~
12 ~~than 1000 and the derivative is greater than 100 % per 0.10 AOD~~. Figure ~~8~~11 presents
13 calculations, similar to Figure ~~7~~9, except that the ~~India land~~large derivatives are excluded
14 from the calculation. Over the ocean and land the means are near 5% and 4% per 0.1 AOD,
15 respectively, for the 9 - 13 km range.

16 Curves similar to Figure ~~8~~11 (not shown), were calculated for each Season of the year.
17 Over land the Winter and Spring curves of the IWC_{shape} means have altitude structure
18 similar to Figure ~~8~~11 in that the means steadily increase as altitude increases. The Fall land
19 means, however, are all near zero. Over the oceans the means are positive above 11 km
20 altitude for all four seasons. The land and ocean seasonal means, however, are not
21 statistically significant to the 2σ level.

22 ~~An alternative way to calculate the means in Figure 8 is to weight the averaging process by~~
23 ~~the number of profiles in each region. This calculation, which includes India derivatives~~
24 ~~(but gives them little weight), again yields means between 5% and 4% per 0.1 AOD over~~
25 ~~ocean and land, respectively.~~

26 ~~Finally, Figure 9~~As discussed in the Introduction, AODs are expected to invigorate
27 convection for low AODs, with saturation apparent at larger AODs. These saturation
28 effects start to occur for AODs near 0.30 and 0.40 as calculated by Rosenfeld et al. (2008)
29 and Koren et al. (2008), respectively. These saturation onset AODs correspond to the third

Formatted: Font: 12 pt, Not Superscript/ Subscript

Formatted: Font: 12 pt, Not Superscript/ Subscript

AOD range (0.35 – 0.45) of our calculations. To quantify the percent of observations which are consistent with this *saturation* scenario, we calculated for each region, season, and altitude, $\Delta IWC(i,j)$ differences

$$\Delta IWC(i,j) = IWC_{shape}(i) - IWC_{shape}(j) \quad (5)$$

where i or j refers to the aerosol bins 1,2,3 (i.e. the three MODIS aerosol bins in Table 1), respectively. If the first difference $\Delta IWC(2,1)$ was positive, and the difference $\Delta IWC(3,2)$ was negative or less than the absolute value of the first difference, then this indicated saturation. With regards to inhibition, this scenario corresponds to the case in which the $\Delta IWC(2,1)$ and $\Delta IWC(3,2)$ values are both negative. Table 4 presents the percentages for which these two scenarios appeared in our calculations based upon the MODIS data. The saturation scenario occurred approximately twice as often as the inhibition scenario. These percentages are for “ideal” outcomes in which both ΔIWC values are used to identify one scenario or the other.

Figure 12 displays the means of PDFs specified by combining the land and ocean IWC_{shape} derivatives, excluding the ~~India-land~~~~largest~~ derivatives, to obtain a *Tropical average*. The means of the shape derivatives are near 5% per 0.1 AOD (as expected from Figure 811), and positive to the 2σ level in the 11 to 15 km altitude range. Also displayed in Figure 912 are means calculated using the IWC_{reg} derivatives, again excluding the ~~India-land~~~~largest~~ derivatives. The means are positive above 9 km altitude, but not statistically significant at the 2σ level. The mean of the IWC_{reg} derivatives in the 5-7 km altitude range is nonzero (i.e. 0.04) but very small.

Another way to look at the derivatives is by graphing PDFs of the derivatives. Figure 13 presents PDFs of the IWC_{shape} derivatives for the AOD, AAOD, and CO data. Derivatives over the ocean and land regions (excluding the largest derivatives) were aggregated for the 7 – 13 altitude range. All PDFs have a main gaussian-like distribution, with several smaller contributions outside of the primary distribution. Averages of the PDFs are indicated at the top of the panels. The arithmetic means of the PDFs are less for the AAOD and CO data than for the AOD data, with positive means for the AOD data, and negative means

Formatted: Font: 12 pt, Not Superscript/ Subscript

Formatted: Font: 12 pt, Not Superscript/ Subscript

1 especially for the CO data. These results are supportive of the assertion that absorptive
2 aerosol tends to inhibit cloud development.

3 Figure 14 presents average IWC_{reg} derivatives for AOD, AAOD, and CO data over ocean
4 and land for all regions, excluding the largest derivatives. For legibility purposes, 1σ
5 confidence limits of the determination of the means are given by the horizontal lines. The
6 CO means over land and ocean are negative for the 7 – 15 km altitude range.

7 Finally, Figure 15 is similar to Figure 14 except that average shape derivatives are
8 presented. The AAOD and CO shape derivative means are less than the AOD means both
9 over ocean and land for the 9 – 15 km altitude range. These results are supportive of the
10 assertion that absorptive aerosol tends to inhibit cloud development. It is notable in both
11 Figures 14 and 15 that the size of the mean derivatives are fairly small, with values mostly
12 between -15 and 5%.

14 **5 Discussion**

15 ~~The calculations above are supportive of a small positive signed cloud invigoration effect.~~
16 IWC increases slightly on average for deep convective clouds above the freezing level as
17 AODs increase. ~~The Figure 7 means of the IWC_{shape} PDF, based upon all Tropical regions,~~
18 ~~indicates mean IWC_{shape} derivatives over the ocean and land are near 5% and 10–20% per~~
19 ~~0.1 AOD in the 9–13 km altitude range, respectively. The derivatives are positive to the~~
20 ~~2σ level for the 9–11 and 13–15 km altitude ranges over land. If the largest derivatives (see~~
21 ~~Figure 5, those over India), are excluded from the processing (since the India derivatives~~
22 ~~are very much larger than the other derivatives, and many less cloudy scenes are observed~~
23 ~~over India due to the comparatively smaller geographical size of India), then the IWC_{shape}~~
24 ~~land mean derivative is near 4% (see Figure 8).~~

25 The Tropical average means (Figure 912), calculated using combined ocean and land
26 IWC_{shape} derivatives (excluding ~~mainland India~~ the largest derivatives) are near 5% per
27 0.1 AOD above 9 km altitude, and positive to the 2σ level in the 11 – 15 km range. The

Formatted: Font: 12 pt, Not Superscript/ Subscript

5% per 0.1 AOD value is similar to the ~~observed-previously determined~~ 7% per 0.1 AOD value ~~observed over the equatorial Atlantic region~~ (corresponding to the cloud top pressure data of Figure 6 from Koren et al., 2010), and similar to the 3% – 5% increase in medium and high cloud tops calculated by Storer and van den Heever (2013), but substantially less than the ~127% / 0.1 AOD change in the IWC profile indicated by the bin microphysics calculations presented in Figure 6 of Lebo and Seinfeld (2011).

As discussed above, the IWC_{reg} average profiles are calculated without normalization at 5 km altitude. The IWC_{reg} means ~~(excluding India)~~ in Figure 12 are positive above 9 km but not statistically significant at the 2 σ level. The lack of statistical significance is similar to the conclusions of Wall, Zipser, and Liu (2014). One is struck by the fact that our study and that of Wall, Zipser, and Liu (2014) both yield ~~small~~ inconclusive aerosol indirect effects when many years of data are processed.

~~Generally,~~ Figure 57 imparts an important lesson – the scatter in the measured derivatives decreases ~~for a region when~~ as the number of observed profiles in the ~~region~~ various regions increases. We interpret Figure 57 as follows. Changes in IWC vertical structure are due to both aerosol and cloud dynamic influences. For a specific region, a relatively small number of profiles will not likely sample the PDFs of all variables (aerosol and cloud dynamic variables such as surface and 500 hPa relative humidity, CAPE, wind shear, etc) as completely as for the case in which a larger number of profiles are considered. Differences in the average IWC_{reg} profiles at different AODs can be due to differences in cloud dynamic differences, to a greater extent than to the AOD difference, depending upon circumstance, if the number of observed profiles is relatively small. A negative (or large positive) derivative could be due to a change in cloud dynamic influences and not the AOD change. In addition, the CloudSat/CALIPSO observational 2D “curtains” slice through a cloudy region. If the sampling of ~~the~~ 3D cloudy regions with respect to low and high regions of IWC is not consistently similar for the e.g. three bins of AOD, then a sampling issue arises. This sampling consideration becomes less of an issue when the number of observed profiles increases.

Formatted: Font: 12 pt, Not Superscript/ Subscript

Formatted: Font: 12 pt, Not Superscript/ Subscript

Formatted: Font: 12 pt, Not Superscript/ Subscript

1 Interest in the cloud invigoration process is of course important due to its consequences in
2 regard to the radiative effects of aerosol indirect effects – perturbations in cloud vertical
3 structure due to changes in aerosol translate into perturbations in the radiative effects of
4 clouds upon climate. Understanding the effects of aerosols upon cloud structure is a
5 necessary step towards understanding the radiative effects. Global calculations which
6 average regional and seasonal perturbations of cloud structure over many years are of
7 interest since they yield a grand ensemble average that fully samples the PDFs of the
8 aerosol and cloud dynamic variables.

9 It is apparent from our calculations that both *invigoration* processes (Rosenfield et al. 2008,
10 Koren et al. 2008) and *inhibition* processes (Ramanathan et al., 2005; Ramanathan et al.,
11 2007) are expressed in our long term derivatives which indicate that IWC can both increase
12 or decrease as AOD increases. Changes in MODIS IWCshape profiles did indicate
13 saturation effects as discussed by Koren et al. (2008). Saturation effects, in which an
14 increase in IWC is followed by a small increase or decrease in IWC, was present 32% of
15 the time (the average of the 1st and 2nd columns of Table 4). The means of the PDFs
16 presented in Figure 13, and the means of the IWCshape derivatives presented in Figure 15
17 are also supportive of the assertion that absorptive aerosol can *inhibit* cloud development.
18 Inhibition effects were present 17% of the time (the average of 3rd and 4th columns of Table
19 4). The saturation scenario for MODIS data occurred approximately twice as often as the
20 inhibition scenario.

21 Cloud adjacency (i.e. 3D radiative transfer) issues are real, but the impact in our particular
22 calculations is a second order effect. The 3D cloud adjacency effects appear not to be a
23 major impediment in regard to calculation of aerosol-cloud indirect effects, if the AOD bin
24 ~~ranges~~ ranges are fairly wide compared to the size of the 3D effect (see Figure 46). The
25 variations in the IWC_{reg} land derivatives in Table 42 for the “all AOD”, 2, and 4 pixel-
26 unit cases is ~~much~~ smaller than the altitude variations in the derivatives. We place an AOD
27 into one of three AOD bin ranges. An e.g. 2% AOD correction (see Figure 46) due to cloud
28 adjacency effects does not likely move the AOD from one bin range to another. As
29 remarked above, the number of 1°x1° AODs decrease as the pixel-distance unit increases,
30 ~~and with.~~ With the “all AOD” and 2 pixel-distance AODs giving similar derivatives over

Formatted: Font: 12 pt, Not Superscript/ Subscript

land in the right-hand portion of Table 42, and with the similarity in the curves presented in Figure 8 for the three screening cases, the necessity to apply the pixel-distance correction is debatable.

In conclusion, the literature of observed and modeled aerosol-cloud indirect effects is characterized by a range of results of different signed outcomes, including this study. This is due to the fact that numerous variables and many other physical considerations can influence whether a positive or negative effect is measured. For example, In Figure 15 there is a stark contrast between the positive AOD derivatives above 9 km altitude, and the negative CO derivatives. A portion of the contrasting positive and negative results reported in the literature is likely due to whether or not absorptive aerosol is known to stabilize the lowermost several kilometers of temperature profiles, and thus could impact cloud development. In our study we consider all MODIS AODs equally, without attention to the type absent or present in a particular set of aerosol (be it predominantly scattering or absorptive in nature). We will address this issue in follow on calculations, and also extend our calculations to include dynamic variables in the analyses observations.

Acknowledgements

The work discussed in this paper is supported by NASA Grants NNX14AL55G and NNX14AO85G. DARDAR data were provided by NASA/CNES and we thank the ICARE Data and Services Center (<http://www.icare-lille1.fr>) for providing access to the data used in this study. The National Center for Atmospheric Research (NCAR) is supported by the National Science Foundation.

References

Cotton, W., and Coauthors: RAMS 2001: Current status and future directions, Meteor. Atmos. Phys. 82, 5-29, 2003.

- 1 Delanoë, J., and Hogan, R. J.: A variational scheme for retrieving ice cloud properties from
2 combined radar, lidar, and infrared radiometer, *J. Geophys. Res.*, 113, D07204,
3 doi:10.1029/2007JD009000, 2008.
- 4 Delanoë, J., and Hogan, R. J.: Combined CloudSat-CALIPSO-MODIS retrievals of the
5 properties of ice clouds, *J. Geophys. Res.*, 115, D00H29, doi:10.1029/2009JD012346,
6 2010.
- 7 Deng, M., Mace, G. G., Wang, Z., and Lawson, P. R.: Evaluation of Several A-Train Ice
8 Cloud Retrieval Products with In Situ Measurements Collected during the SPARTICUS
9 Campaign, *J. Appl. Met. Clim.*, 52, 1014-1030, 2013.
- 10 [Fan J., Leung, L. R., Rosenfeld, D., Chen, Q., Li, Z., Zhang, J., and Yan, H.:
11 Microphysical effects determine macrophysical response for aerosol impacts on deep
12 convective clouds, *Proceedings of the National Academy of Sciences*, 110\(48\), E4581-
13 E4590, 2013](#)
- 14 Hogan, R. J.: Fast approximate calculation of multiply scattered lidar returns, *Appl. Opt.*,
15 45, 5984–5992, 2006.
- 16 Houze, R.: *Cloud Dynamics*, Elsevier, Amsterdam, 2014.
- 17 [Jiang, J. H., Su, H., Schoeberl, M., Massie, S. T., Colarco, P., Platnick, S., and Livesey, N.
18 J.: Clean and polluted clouds: relationships among pollution, ice cloud and precipitation in
19 South America, *Geophys. Res. Lett.*, 35, L14804, doi:10.1029/2008GL034631, 2008.](#)
- 20 [Jiang, J. H., Su, H., Massie, S. T., Colarco, P. R., Schoeberl, M. R., and Platnick, S.:
21 Aerosol-CO relationship and aerosol effect on Ice cloud particle size: Analyses from Aura
22 Microwave Limb Sounder and Aqua Moderate Resolution Imaging Spectroradiometer
23 observations, *J. Geophys. Res.* 114, D20207, doi:10.1029/2009JD012421, 2009.](#)
- 24 [Koren, I., Martins, J. V., Remer, L. A., and Afargan, H.: Smoke invigoration versus
25 inhibition of clouds over the Amazon. *Science*, 321\(5891\), 946-949, 2008.](#)

1 Koren, I., Feingold, G., and Remer, L. A.: The invigoration of deep convective clouds over
2 the Atlantic: aerosol effect, meteorology or retrieval artifact? *Atmos. Chem. Phys.*, 10,
3 8855-8872, 2010.

4 [Lau, K. M., Kim, M. K., and Kim, K. M: Asian summer monsoon anomalies induced by](#)
5 [aerosol direct forcing: the role of the Tibetan Plateau, 26, 855-864, doi:10.1007/s00382-](#)
6 [006-0114-z, 2006.](#)

7 Lebo, Z. J., and Seinfeld, J. H.: Theoretical basis for convective invigoration due to
8 increased aerosol concentration, *Atmos. Chem. Phys.*, 11, 54-7-5429, 2011.

9 Levy, R. C., Mattoo, S., Munchak, L. A., Remer, L. A., Sayer, A. M., Patadia, F., and Hsu,
10 N. C.: The Collection 6 MODIS aerosol products over land and ocean, *Atmos. Meas. Tech.*,
11 6, 2989-3034, doi:10.5194/amt-6-2989-2013, 2013.

12 Levy, R. C., Mattoo, S., Munchak, L. A., Kleidman, A. R., Patadia, F., and Gupta, P:
13 MODIS Atmosphere Team Webinar Series#2: Overview of Collection 6 Dark-Target
14 aerosol product, http://modis-atmos.gsfc.nasa.gov/products_C006update.html, 2014.

15 Liu, C., and Zipser, E. J.: Diurnal cycles of precipitation, clouds, and lightning in the tropics
16 from 9 years of TRMM observations, *Geophys. Res. Lett.*, 35, L04819,
17 doi:10.1029/2007GL032437, 2008.

18 [Livesey, N. J., et al.: Validation of Aura Microwave Limb Sounder O3 and CO](#)
19 [observations in the upper troposphere and lower stratosphere, *J. Geophys. Res.*, 113,](#)
20 [D15S02, doi:10.1029/2007JD008805, 2008.](#)

21 [Livesey, N. J., Read, W. G., Wagner, P. A., Froidevaux, L., Lambert, A., Manney, G. L.,](#)
22 [Mill'an, L. F., Pumphrey, H. C., Santee, M. L., Schwartz, M. J., Wang, S., Fuller, R. A.,](#)
23 [Jarnot, R. F., Kropf, B. W., and Martinez, E.: Version 4.2x Level 2 data quality and](#)
24 [description document. JPL D-33509 Rev. A, \[http://mls.jpl.nasa.gov/data/v4-\]\(http://mls.jpl.nasa.gov/data/v4-2_data_quality_document.pdf\)](#)
25 [2_data_quality_document.pdf, 2015.](#)

26 Rodgers, C. D: *Inverse Methods for Atmospheric Sounding*. World Scientific, Singapore,
27 2000.

Rosenfeld, D., Lohmann, U., Raga, G. B., O'Dowd, C. D., Kulmala, M., Fuzzi, S., Reissell, A., and Andreae, M. O.: Flood or drought: How do aerosols affect precipitation?, *Science*, 321, 1309– 1313, doi:10.1126/science.1160606, 2008.

Stephens, G. L., Vane, D. G., Boain, R. J., Mace, G. G., Sassen, K., Wang, Z., Illingworth, A. J., O'Connor, E. J., Rossow, W. B., Durden, S. L., Miller, S. D., Austin, R. T., Benedetti, A., Mitrescu, C., and The CloudSat Science Team: THE CLOUDSAT MISSION AND THE A-TRAIN, *Bull. Amer. Meteor. Soc.*, **83**, 1771–1790, doi: <http://dx.doi.org/10.1175/BAMS-83-12-1771>, 2002.

Stocker, T.F., Qin, D., Plattner, G.-K., Alexander, L. V., Allen, S. K., Bindoff, N. L., Bréon, F.-M., Church, J. A., Cubasch, U., Emori, S., Forster, P., Friedlingstein, P., Gillett, N., Gregory, J. M., Hartmann, D. L., Jansen, E., Kirtman, B., Knutti, R., Krishna Kumar, K., Lemke, P., Marotzke, J., Masson-Delmotte, V., Meehl, G. A., Mokhov, I. I., Piao, S., Ramaswamy, S. V., Randall, D., Rhein, M., Rojas, M., Sabine, C., Shindell, D., Talley, L. D., Vaughan, D. G., and Xie, S.-P.: Technical Summary. In: *Climate Change 2013: The Physical Science Basis. Contribution of Working Group I to the Fifth Assessment Report of the Intergovernmental Panel on Climate Change* [Stocker, T.F., Qin, D., Plattner, G.-K., Tignor, M., Allen, S. K., Boschung, J., Nauels, A., Xia, Y., Bex, V., and Midgley, P. M. (eds.)]. Cambridge University Press, Cambridge, United Kingdom and New York, NY, USA, 2013.

Storer, R. L., and van den Heever, S. C.: Microphysical Processes Evident in Aerosol Forcing of Tropical Deep Convective Clouds, *J. Atm. Sci.*, 70, 430-446, 2013.

Tao, W.-K., Chen, J.-P., Li, Z., Wang, C., and Zhang, C.: Impact of aerosols on convective clouds and precipitation, *Rev. Geophys.*, 50, RG2001, doi:10.1029 /2011RG000369, 2012.

Varnai, T., and Marshak, A.: MODIS observations of enhanced clear sky reflectance near clouds, *Geophys. Res. Lett.*, 36, L06807, doi:10.1029/2008GL037089, 2009.

Veihelmann, B. et al.: Simulation study of the aerosol information content in OMI spectral reflectance measurements, *Atmos. Chem. Phys.*, 7, 3115-3127, 2007.

1 [Veihelmann, B., and Veefkind, J. P.: knmi.nl/omi/research/product](http://knmi.nl/omi/research/product)
2 [/product_generator.php?info=page&product=aerosol&flavour=OMAERO&long=Aerosol](http://product_generator.php?info=page&product=aerosol&flavour=OMAERO&long=Aerosol)
3 [absorption optical thickness and Aerosol types, 2009.](#)

4 Wall, C., Zipser, E., and Liu, C.: An Investigation of the Aerosol Indirect Effect on
5 convective Intensity Using Satellite Observations, *J. Atmos. Sci.*, 71, 430-447, 2014.

6 Winker, D. M., Pelon, J., Coakley Jr., J. A., Ackerman, S. A., Charlson, R. J., Colarco, P.
7 R., Flamant, P., Fu, Q., Hoff, R. M., Kittaka, C., Kubar, T. L., Le Treut, H., McCormick,
8 M. P., Mégie, G., Poole, L., Powell, K., Trepte, C., Vaughan, M. A., and Wielicki, B. A.:
9 The CALIPSO Mission: A Global 3D View of Aerosols and Clouds. *Bull. Amer. Meteor.*
10 *Soc.*, 91, 1211–1229. doi: <http://dx.doi.org/10.1175/2010BAMS3009.1> , 2010.

11 ~~Varnai, T., and Marshak, A.: MODIS observations of enhanced clear sky reflectance near~~
12 ~~clouds, *Geophys. Res. Lett.*, 36, L06807, doi:10.1029/2008GL037089, 2009.~~

13 Zhang, J., Reid, J. S., and Holben, B. N.: An analysis of potential cloud artifacts in MODIS
14 over ocean aerosol optical thickness products, *Geophys. Res. Lett.*, 32, L15803,
15 doi:10.1029/2005GL023254, 2005.

Table 1. AOD, AAOD, and 215 hPa CO bins used in this study

<u>Bin</u>	<u>AOD</u>	<u>OMI AAOD</u>	<u>MLS CO</u>
<u>1</u>	<u>0.01 – 0.15</u>	<u>0.001 - 0.01</u>	<u>10 – 80 ppbv</u>
<u>2</u>	<u>0.15 – 0.30</u>	<u>0.01 – 0.04</u>	<u>80 - 120</u>
<u>3</u>	<u>0.30 – 0.45</u>	<u>0.04 – 0.10</u>	<u>120 - 150</u>

Table 2. Average IWCreg derivatives over ocean and land (in % / 0.1 AOD units) expressed as a function of average pixel-distance values used to derive the AOD fields.

<u>Altitude</u> (km)	<u>Ocean</u>			<u>Land</u>		
	0	2	4 pixels	0	2	4 pixels
13-15	4.4	5.1	-3.8	2.8	1.7	1.7
	(47	42	27)	(31	31	28)
11-13	0.6	-0.3	2.8	23.1	23.5	15.8
	(53	53	46)	(36	36	34)
9-11	-0.9	-0.2	-0.5	18.0	18.0	19.1
	(54	54	48)	(36	36	36)
7-9	-1.7	-0.2	0.5	6.4 5	6.8	6.6
	(54	55	48)	(36	36	36)
5-7	0.4	0.9	1.9	1.7	1.6	1.6
	(54	54	48)	(36	36	36)

~~2-pixels is for AOD to cloud pixel distances ≥ 2~~

~~Numbers in () are the number of regional and seasonal derivatives used to define the averages.~~

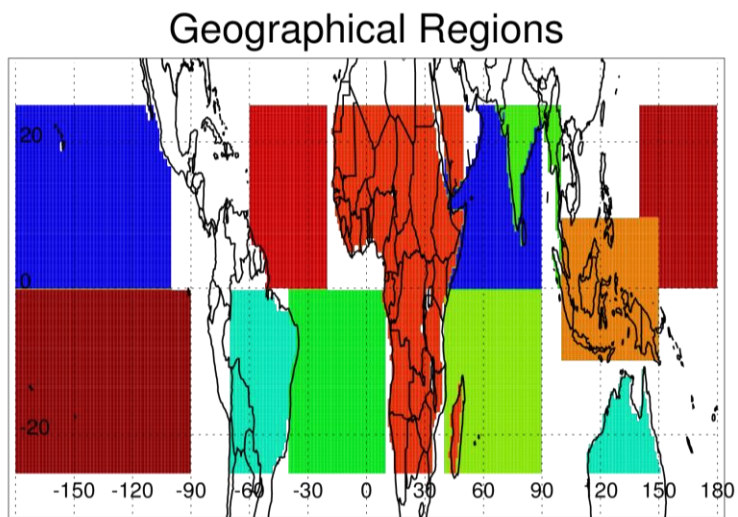
Table 23. Average IWCreg and IWCshape derivatives over ocean and land (expressed in % change in IWC / 0.1 AOD units)

Altitude (km)	Ocean			Land		
	IWCreg	Shape	IWCshape Rnd	IWCreg	Shape	IWCshape Rnd
13-15	4.4	7.4	2.0	2.8	4.6	1.6
11-13	0.6	5.3	2.8	23.1	23.8	1.2
9-11	-0.9	5.4	2.42	18.0	14.5	0.1
7-9	-1.7	-0.2	1.2	6.5	3.0	-0.7
5-7	0.4	0.0	0.0	1.7	0.0	0.0

Rnd – same as IWCshape, with random MODIS AOD values used in the calculation.

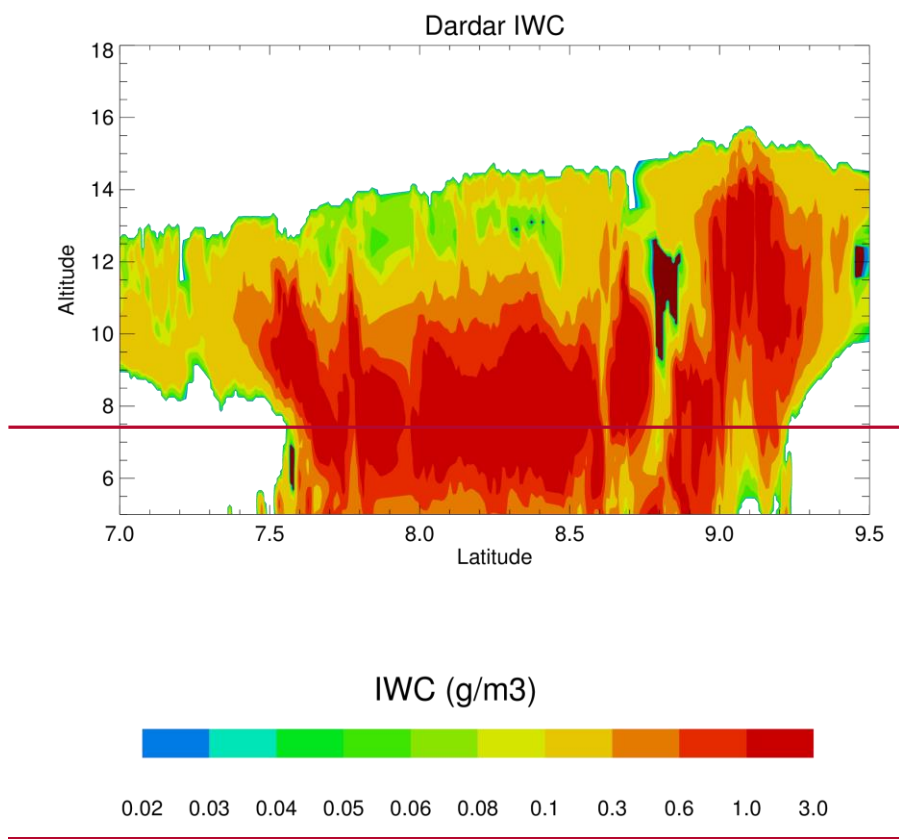
Table 4. Percent of the observations indicating saturation and inhibition effects as MODIS AODs increase.

<u>Altitude</u> <u>(km)</u>	<u>Saturation</u>		<u>Inhibition</u>	
	<u>Ocean</u>	<u>Land</u>	<u>Ocean</u>	<u>Land</u>
<u>13-15</u>	44	27	22	13
<u>11-13</u>	41	50	26	11
<u>9-11</u>	30	50	26	11
<u>7-9</u>	33	44	18	39



1

2 Figure 1. Geographical Tropical regions over land and ocean.



1

2

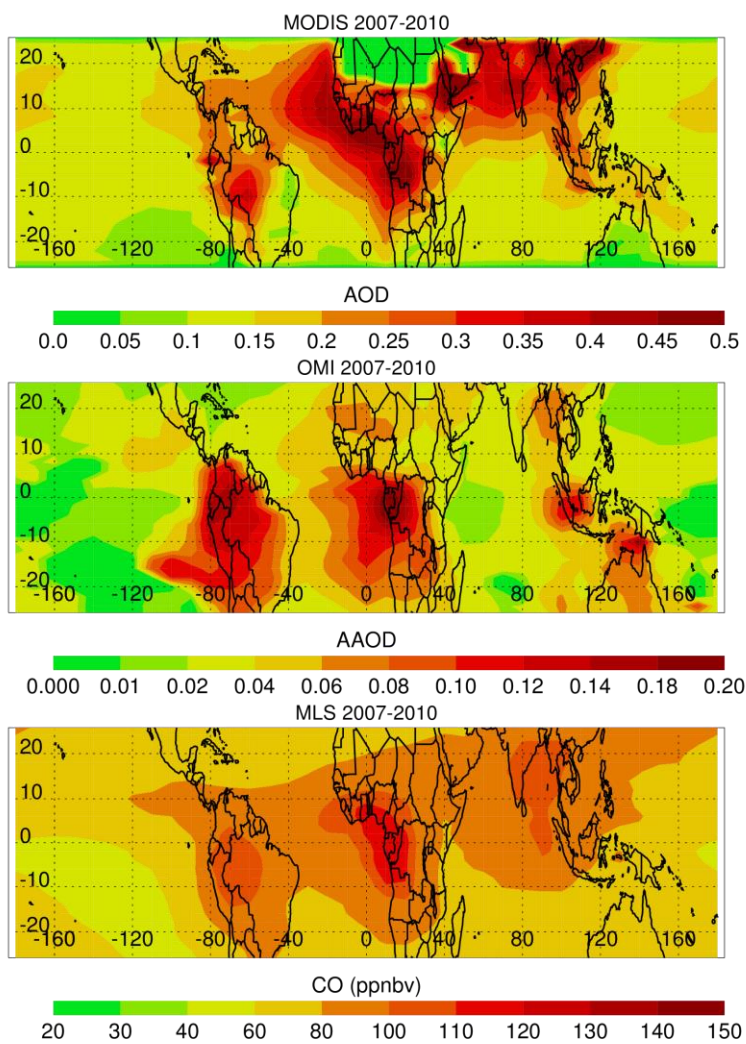
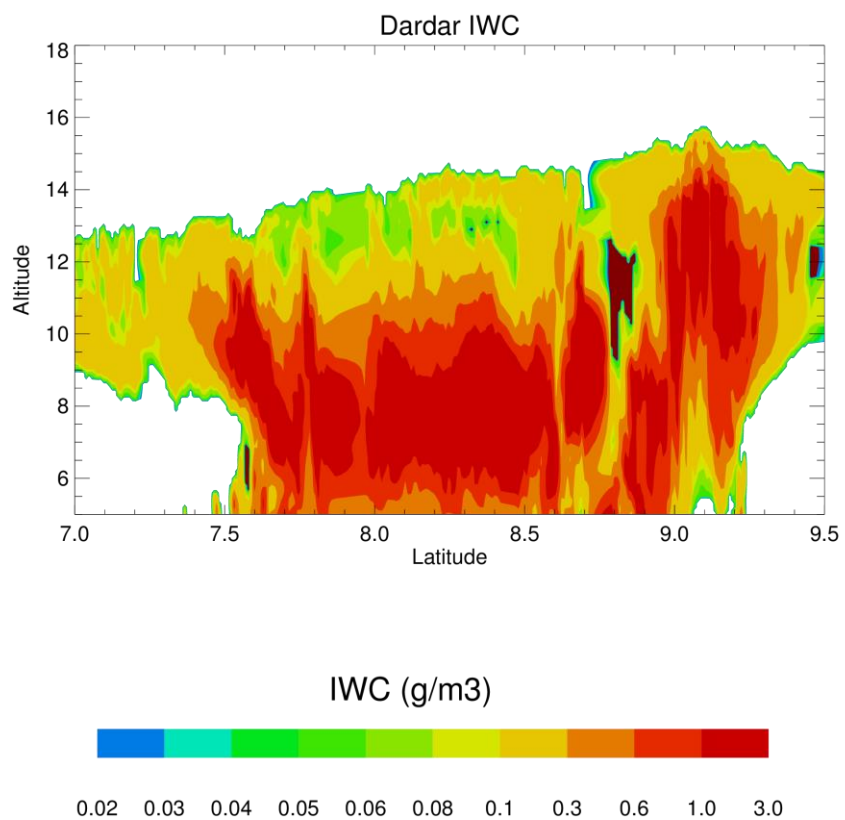
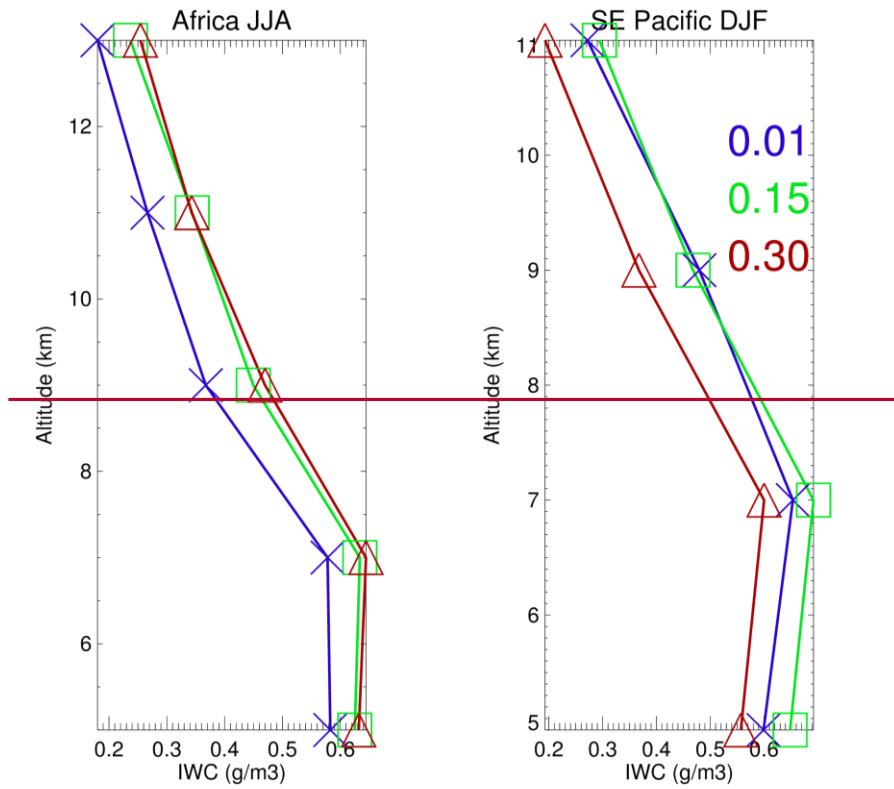


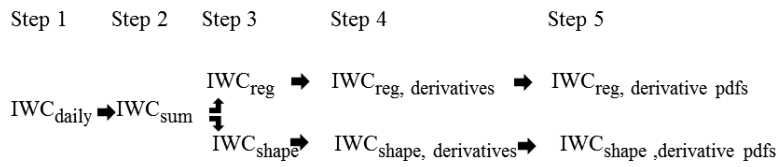
Figure 2. Average MODIS AOD, OMI AAOD, and MLS CO at 215 hPa for 2007-2010.



- 1
- 2 [Figure 3.](#) DARDAR IWC structure of a tropical cloudy region observed on July 10, 2007.



1



2

3 Figure 34. Summary of the processing steps.

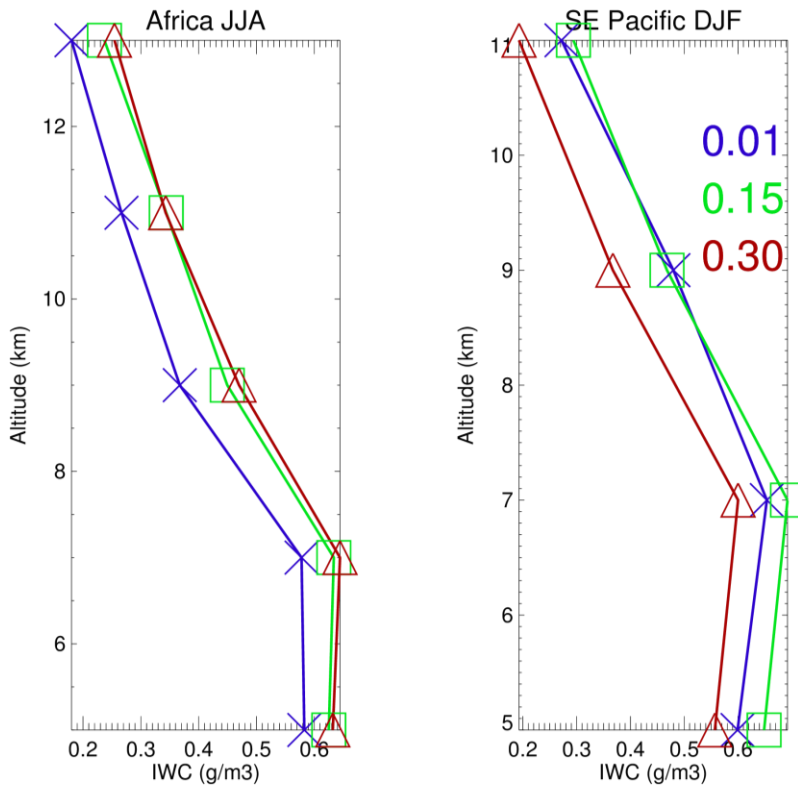
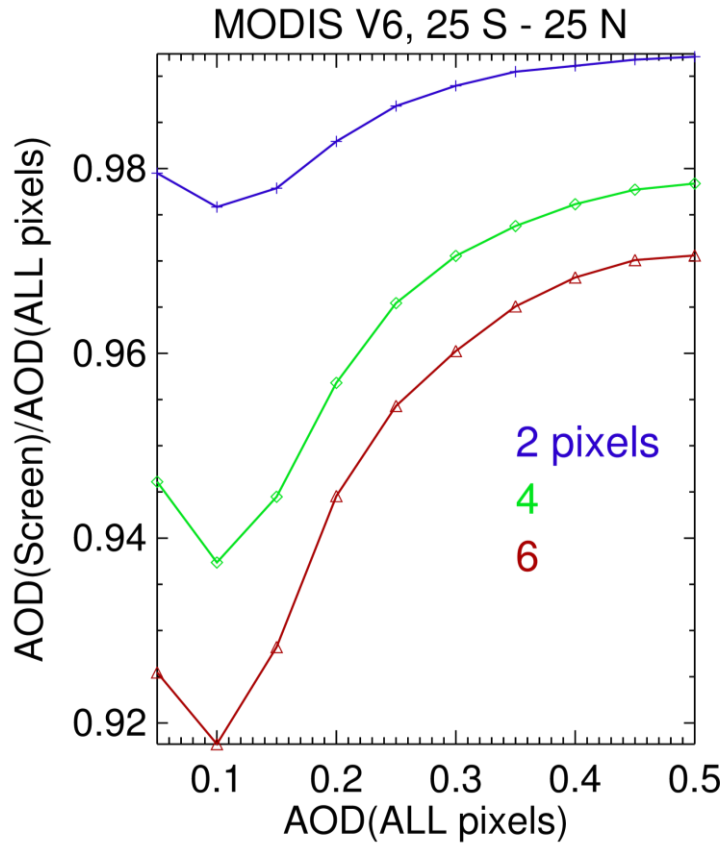
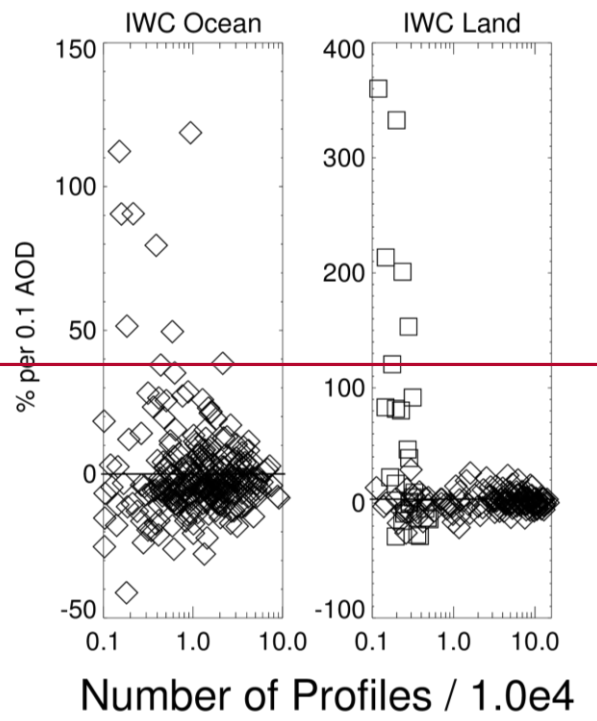


Figure 5. Average IWC_{reg} vertical profiles over SE Pacific during December-January-February and over Africa during June-July-August for MODIS aerosol bins with lower bin limits of 0.01, 0.15, and 0.30. Data has been averaged into 2 km bins of vertical altitude.



1

2 Figure 46. Curves of $1^\circ \times 1^\circ$ MODIS V6 AOD averages, calculated with and without cloud
 3 pixel-distance screening. X axis AOD values are calculated using all MODIS AOD data,
 4 and Y axis AODs are calculated by averaging AODs such that the AODs in the $1^\circ \times 1^\circ$
 5 geographical area are at 2, 4, and 6 pixel-distances from clouds. Data from 2007 – 2010,
 6 for $25^\circ \text{ S} - 25^\circ \text{ N}$, is used.



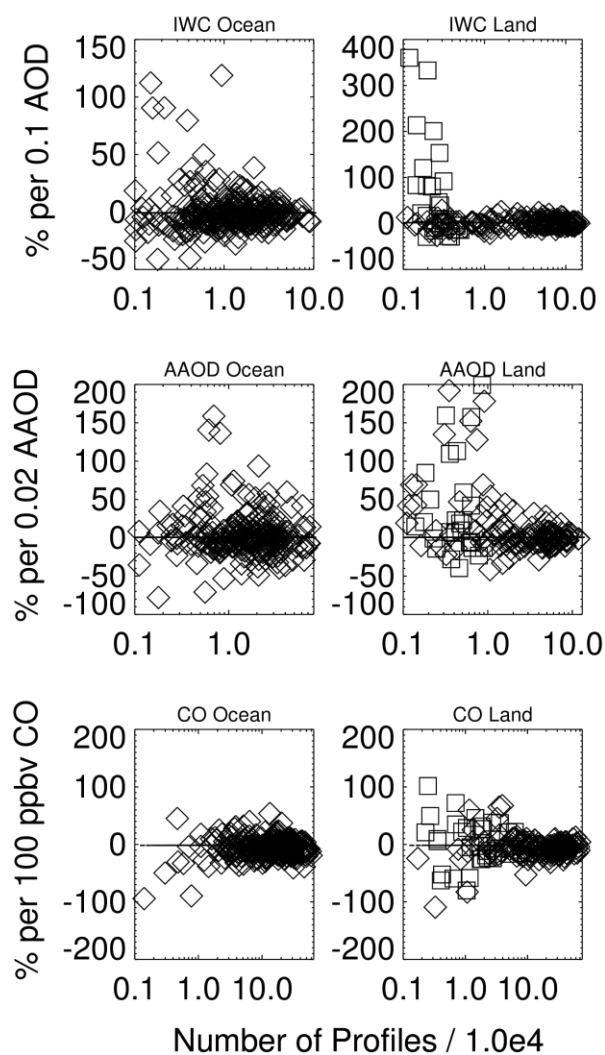
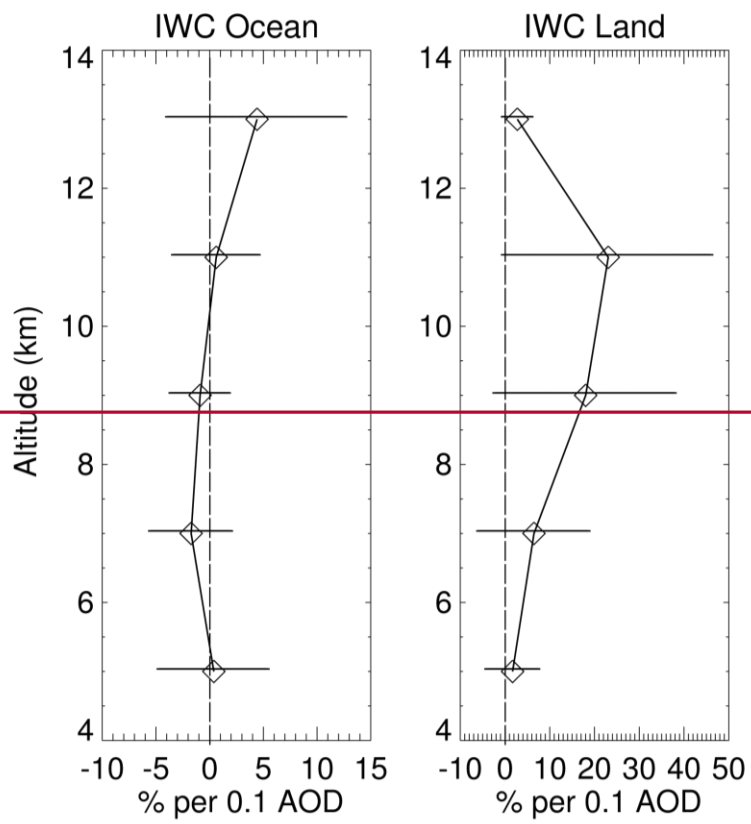


Figure 57. Statistical distribution of IWC_{reg} derivatives between 5 and 15 km altitude for individual regions and seasons as a function of the number of profiles used to define each derivative. Derivatives over mainland India are assigned a square symbol.

Formatted: Font: 12 pt, Not Superscript/ Subscript



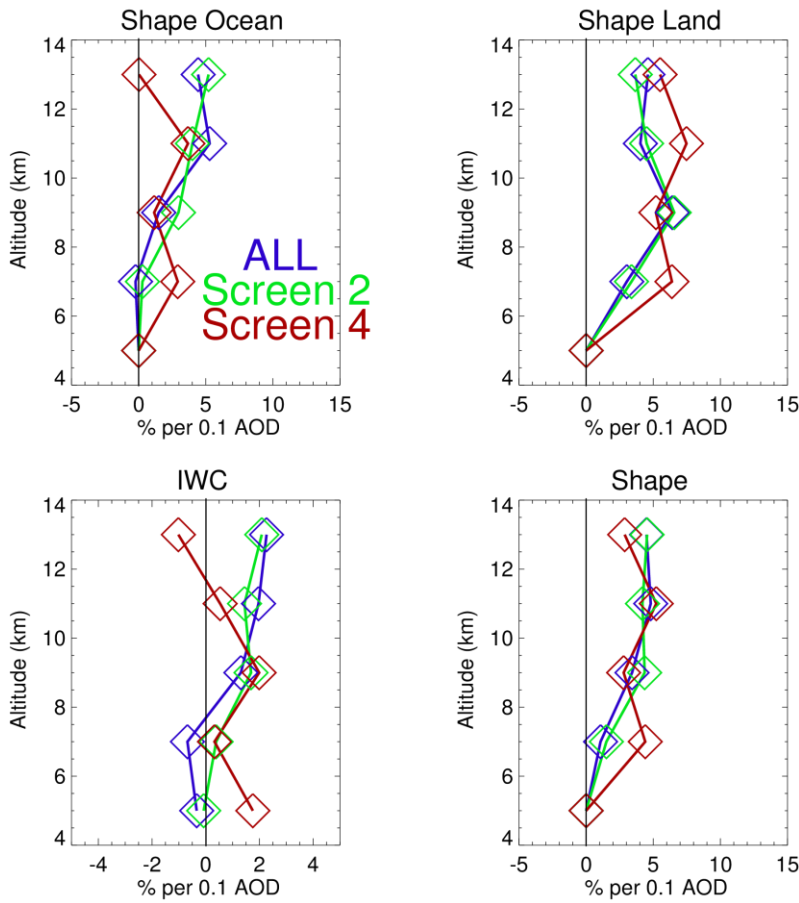


Figure 8. Curves of means of IWCreg and IWCshape PDFs illustrating the sensitivity to the cloud-pixel distance AOD fields. “ALL” refers to the “All AOD” case, and corresponds to curves presented later in the text (i.e. Figures 11 and 12).

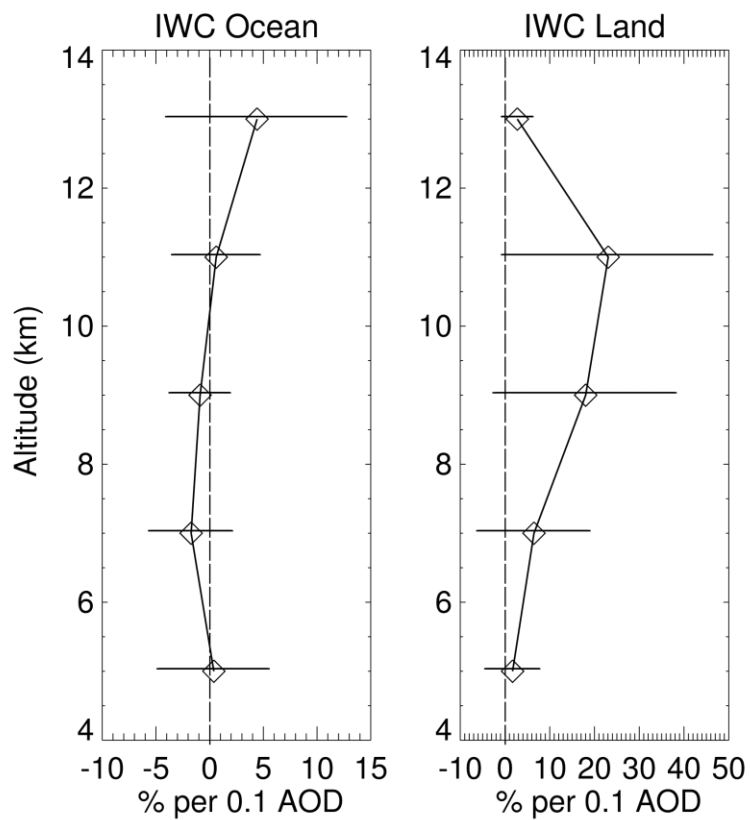
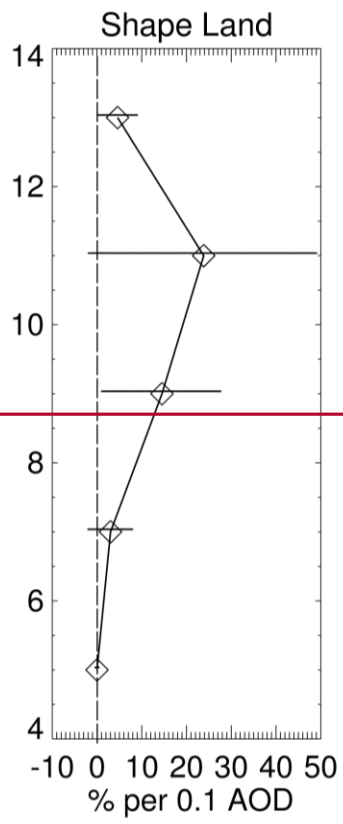
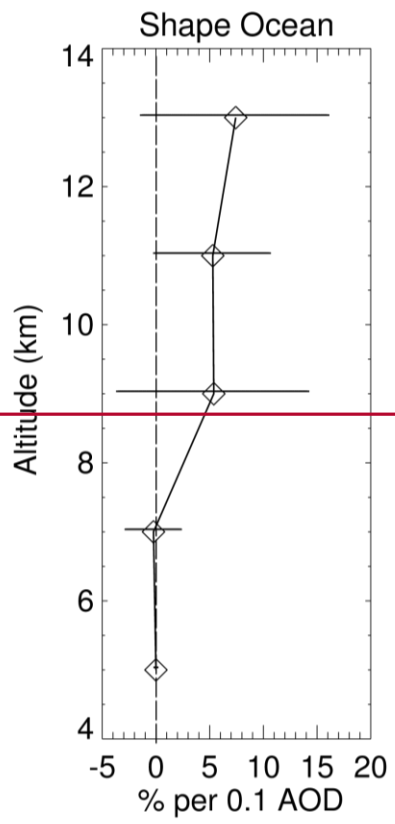


Figure 9. Vertical profiles of the means of the PDFs of IWC_{reg} derivatives for individual regions and seasons based upon DARDAR IWC profiles, and MODIS AOD data for the “all AOD” case. Mean 95% confidence (2σ) limits are indicated by the horizontal lines. The symbol at 5 km denotes the average for the 5-7 km altitude range.

Formatted: Font: 12 pt, Not Superscript/ Subscript



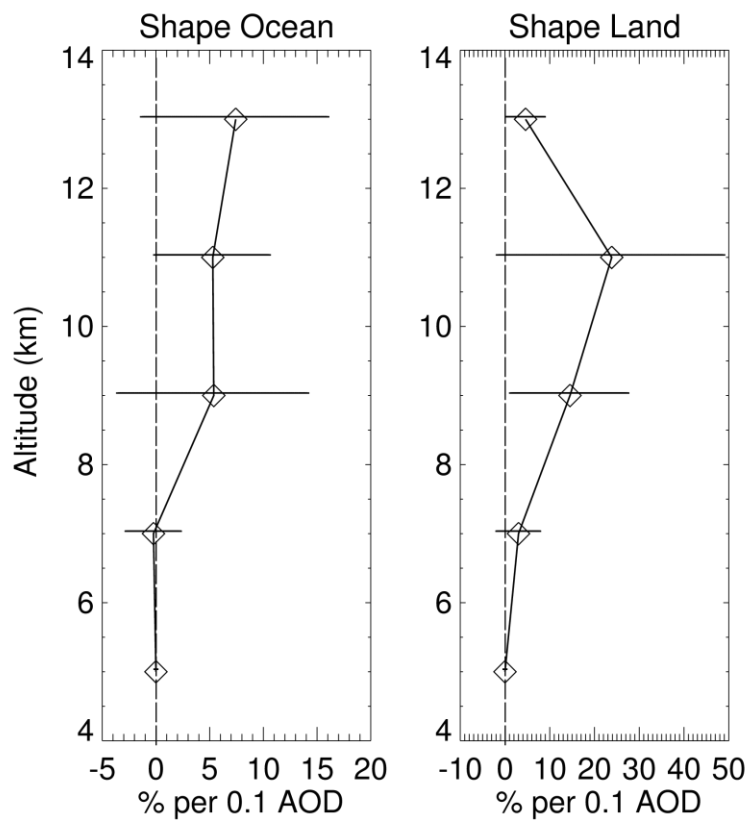
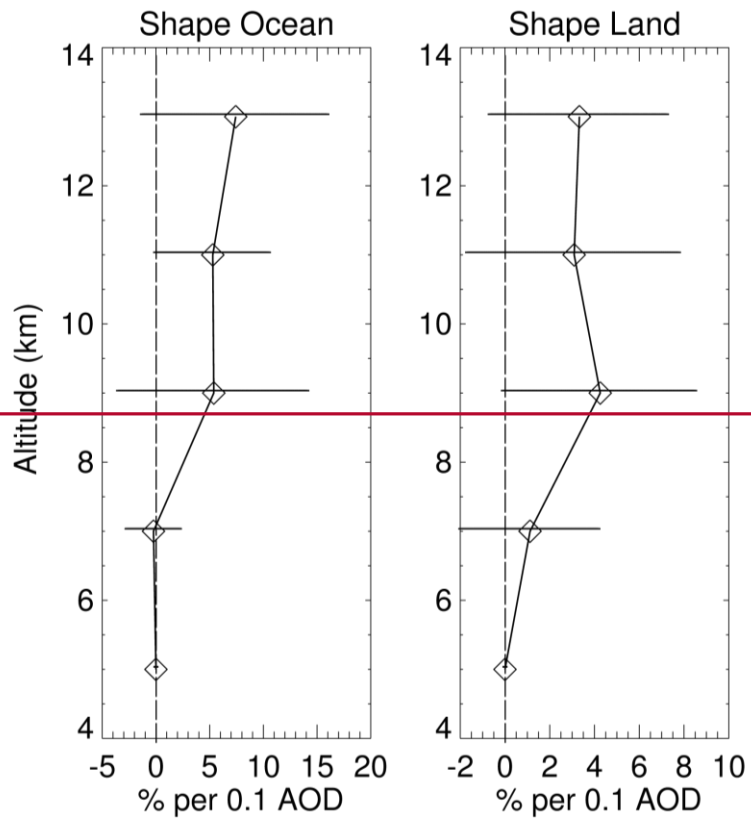
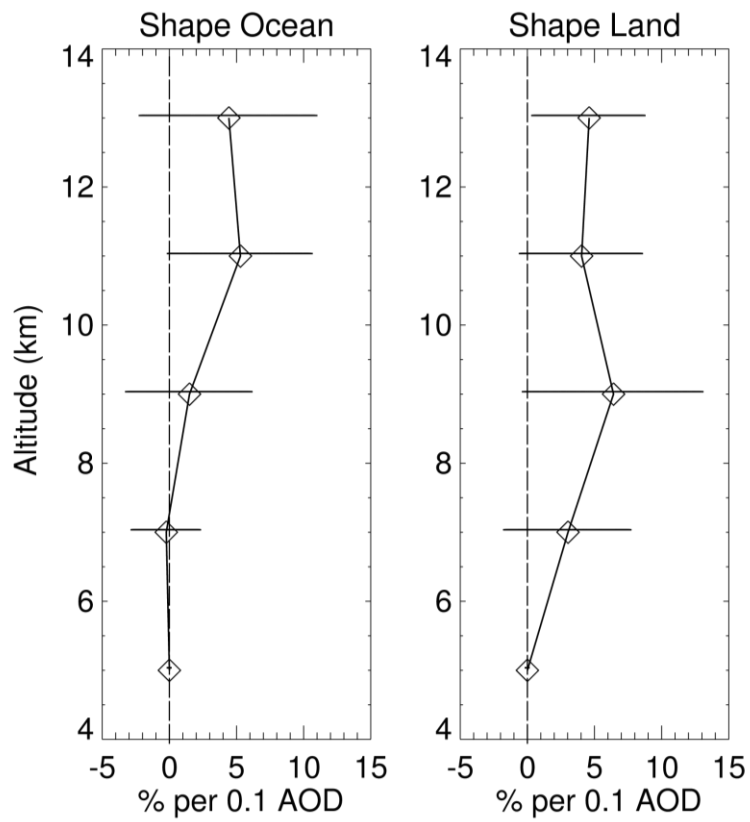


Figure 7.10. Vertical profiles of the means of the IWC_{shape} regional and seasonal derivatives. MODIS “all AOD” data are used. Mean 95% confidence (2σ) limits are indicated by the horizontal lines.

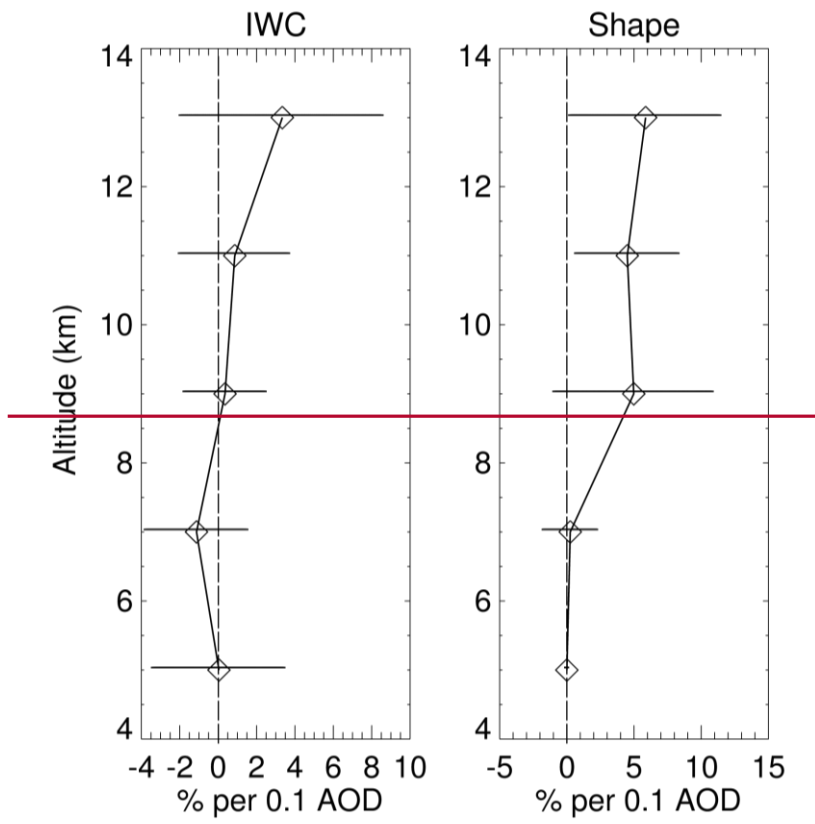
Formatted: Font: 12 pt, Not Superscript/ Subscript



1



- 1
- 2 Figure 811. Same as Figure 79 except that ~~India land~~ IWC_{shape} derivatives less than 100 %
- 3 per 0.1 AOD are excluded from the averaging process.



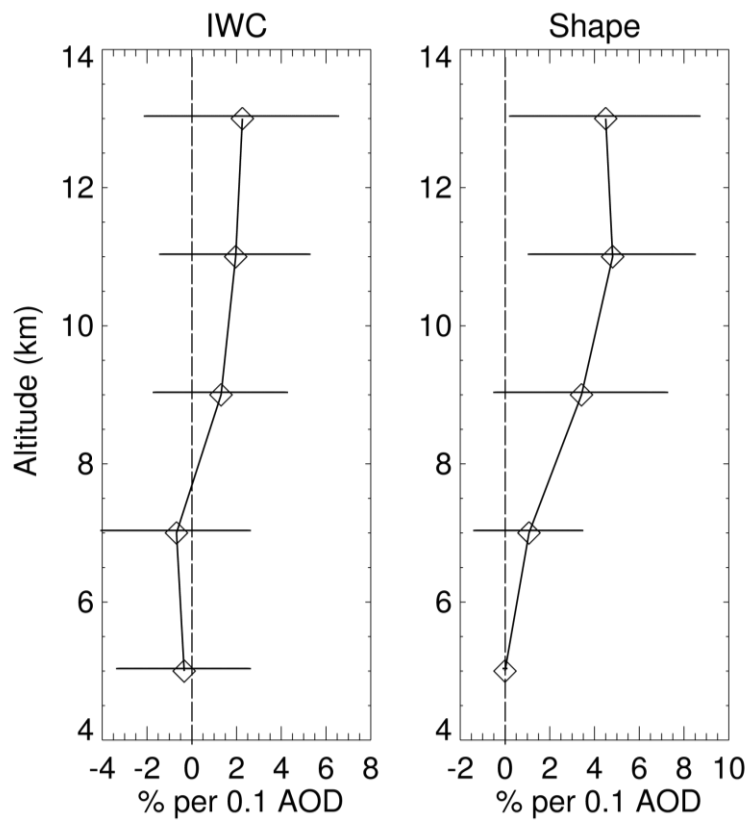


Figure 912. Means of PDFs of IWC_{reg} and IWC_{shape} derivatives over ocean and land, excluding India land derivatives greater than 100 % per 0.1 AOD. Mean 95% confidence limits, given by the horizontal lines, indicate that IWC_{shape} means are positive to the 2σ level for the 11–15 km altitude range.

Formatted: Font: 12 pt, Not Superscript/ Subscript

Formatted: Font: 12 pt, Not Superscript/ Subscript

Formatted: Font: 12 pt, Not Superscript/ Subscript

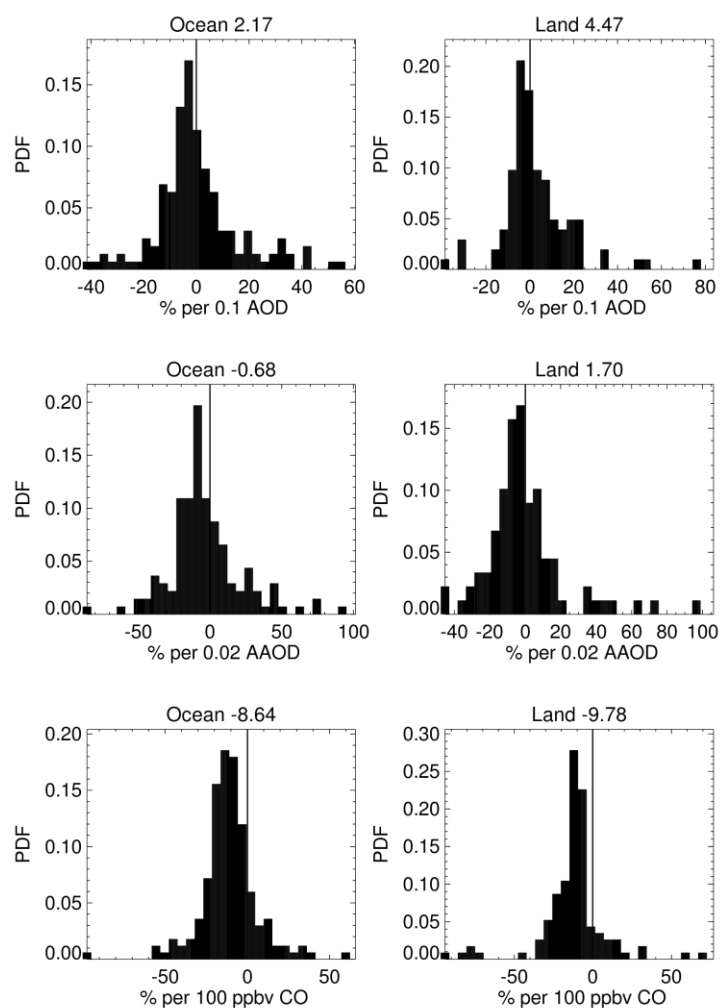
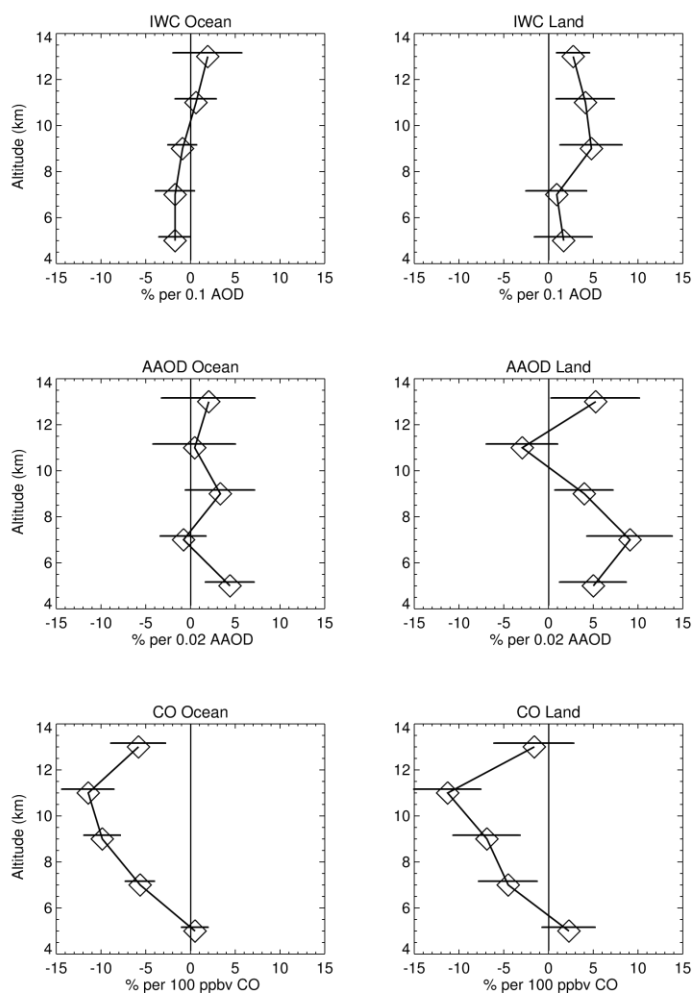


Figure 13. Histograms of IWCshape derivatives for AOD, AAOD, and CO bins, when the derivatives are less than 100 % per 0.10 AOD, 100 % per 0.02 AAOD, and 100% per 100 ppbv CO, respectively. Means of the distributions are indicated by the numbers in each panel's title. Averages pertain to the 7 – 15 km altitude range.



1
2 Figure 14. Average IWC_{reg} derivatives over ocean and land for AOD, AAOD, and CO.
3 Derivatives were used when they were less than 100 % per 0.10 AOD, 100 % per 0.02
4 AAOD, and 100% per 100 ppbv CO. Confidence limits (1σ) of the determination of the
5 means are indicated by the horizontal bars.

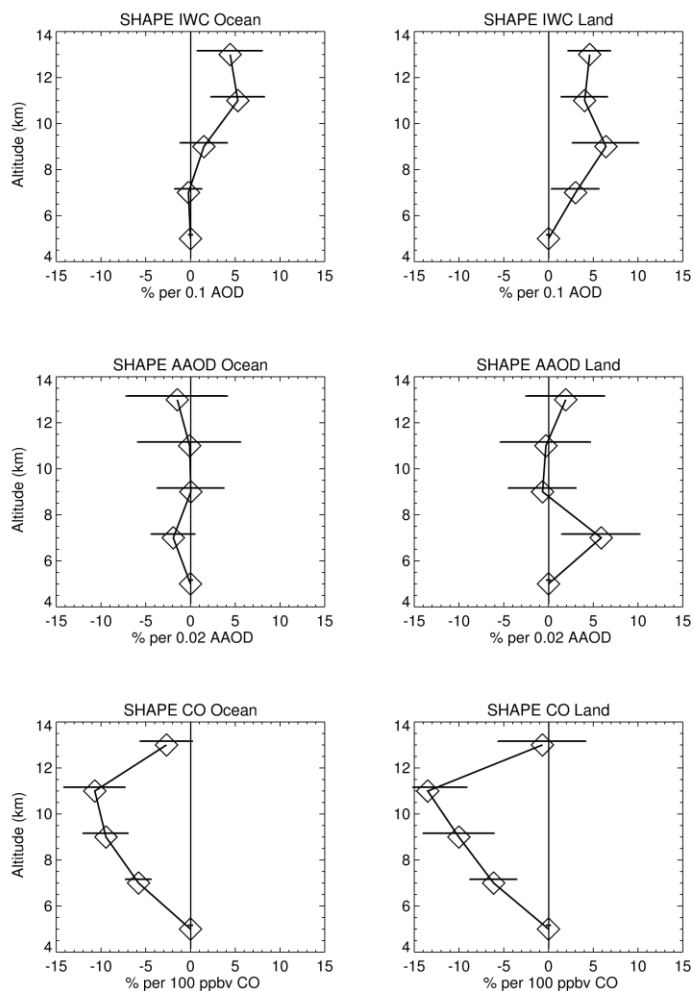


Figure 15. Average IWCshape derivatives over ocean and land for AOD, AAOD, and CO. Derivatives were used when they were less than 100 % per 0.10 AOD, 100 % per 0.02 AAOD, and 100% per 100 ppbv CO. Confidence limits (1σ) of the determination of the means are indicated by the horizontal bars.